

N₂- and (H₂+He)-broadened cross sections of benzene (C₆H₆) in the 7–15 μm region for the Titan and jovian atmospheres



Keeyoon Sung*, Geoffrey C. Toon, Timothy J. Crawford

Jet Propulsion Laboratory, 4800 Oak Grove, California Institute of Technology, Pasadena, CA 91109, United States

ARTICLE INFO

Article history:

Received 31 August 2015

Revised 31 December 2015

Accepted 10 January 2016

Available online 21 January 2016

Keywords:

Benzene (C₆H₆) cross section

Titan atmosphere

FT-IR measurements

Pseudolines

ABSTRACT

In support of atmospheric remote sensing of Titan and jovian planets, we measured absorption cross sections of benzene (C₆H₆) in the 7–15 μm region at temperatures between 235 K and 297 K. For this, high-resolution laboratory spectra of C₆H₆ were obtained using two cold cells (80 cm and 2.07 cm path length) configured to a high resolution Fourier-transform infrared (FT-IR) spectrometer, Bruker IFS-125HR, at the Jet Propulsion Laboratory (JPL). The spectrum sets include 15 pure and 15 N₂-broadened benzene spectra in the 630–1534 cm⁻¹ region, along with four additional spectra broadened by an H₂(85%) and He(15%) gas mixture for the 630–740 cm⁻¹ region. From these spectra, temperature dependent benzene cross sections were obtained for gas phase benzene in the presence of N₂ and (H₂+He) at ambient pressures and temperatures down to 235 K.

In addition, we generated two independent sets of pseudolines: one of N₂-broadened benzene for Titan and the other of (H₂+He)-broadened benzene for jovian planets. It is shown that the benzene pseudolines can reproduce the observed features to ~ 5% in transmittance, including the continuum-like absorption formed by numerous overlapping weak and hot band transitions. Based on the pseudoline parameters, the integrated band intensities at 296 K for the three strongest bands in the region were measured to be 177.0(73), 14.0(10), 27.2(9) × 10⁻¹⁷ cm⁻¹/(molecule·cm⁻²) in the region of ν₄ at 674 cm⁻¹, ν₁₄ at 1038.267, and ν₁₃ at 1483.985 cm⁻¹, respectively, from the combined set of pure and N₂-broadened benzene spectra. For the (H₂+He) mixture-broadened benzene spectra, the integrated band intensity for ν₄ band in the 630–735 cm⁻¹ region was measured to be 168.8(17) × 10⁻¹⁷ cm⁻¹/(molecule·cm⁻²) at 296 K, which is in agreement with the intensity derived from the N₂-broadened benzene spectra within the combined measurement uncertainties. The results from this work show an excellent agreement (2%) with one of the latest experimental studies by Rinsland et al. (2008). Furthermore, additional characteristics carried by the pseudolines approach are discussed. Finally, we provide the two sets of pseudo line list (PLL) as electronic supplements.

© 2016 Elsevier Inc. All rights reserved.

1. Introduction

Benzene (C₆H₆) is a non-methane hydrocarbon (NMHC) observed in the Earth's atmosphere (Doskey and Gaffney, 1992). It is indeed one of the most abundant aromatic hydrocarbons in urban atmospheres. Interestingly, benzene has been identified in the atmosphere of cold giant planets (Jupiter and Saturn) and Titan. It was first detected by Kim et al. (1985) by observing unidentified emission features near 674 cm⁻¹ in Voyager IRIS spectra over the northern aurora region of Jupiter, from which the abundance was estimated to be 1 – 4 × 10⁻⁹ in the polar region. The benzene emission features were later observed in the

upper atmosphere of Jupiter and Saturn (Bézard et al., 2001) and in the stratosphere of Titan (Coustenis et al., 2003) from the Infrared Space Observatory (ISO)/SWS spectra. In Titan's atmosphere, the benzene abundance was deduced to be 4 × 10⁻¹⁰ from the emission features near 674–678 cm⁻¹ using the line intensity of benzene in the ν₄ band reported by Dang-Nhu et al. (1989) and Dang-Nhu and Pliva (1989). Later, Coustenis et al. (2010) reported an extensive study on Titan atmospheric composition from Cassini/CIRS spectra, in which the same ν₄ band features at 674 cm⁻¹ were used for benzene. These observations of benzene were also supported by abundant ions peaking at 78 amu recorded by the mass spectrometer on the Galileo probe (Niemann et al., 1998) and Cassini's ion detections in Titan's ionosphere (Waite et al., 2007; Vuitton et al., 2008; Cui et al., 2009).

Observation of benzene is significant in the understanding the composition and evolution of planetary atmospheres. Benzene is

* Corresponding author. Tel.: +1 818 354 5144.

E-mail address: ksung@jpl.nasa.gov, keeyoonsung@gmail.com (K. Sung).

suggested to be one of the products stemming from hydrocarbon photochemistry initiated by the photodissociation of CH_4 in the upper atmosphere (Wong et al., 2000, 2003). Therefore, benzene has been long predicted to be present on Titan (Raulin et al., 1982; Yung et al., 1984; Thompson et al., 1991; Wilson et al., 2002) or modeled in the photochemistry occurring in the Jovian stratospheres (Moses, et al., 2000; Moses and Greathouse, 2005). Benzene is a precursor for even heavier hydrocarbons, such as polycyclic aromatic hydrocarbons (PAHs) – in fact, benzene itself is the simplest aromatic hydrocarbon. The formation of PAHs through benzene is believed to be the major pathway for aerosol formation in the stratospheres of Jupiter and Titan (Wilson et al., 2002, 2003; Wilson and Treya 2004). Finally, the benzene mixing ratio is observed to be highly correlated with auroral regions of Jupiter and atmospheric haze in Titan (Kim et al., 1985; Yoon et al., 2014).

The detection of benzene in Jupiter's stratosphere in the 1980's was followed by several laboratory studies of benzene spectroscopy in the mid infrared region (Raulin et al., 1990; Khlifi et al., 1992; Akiyama et al., 1989; di Lonardo et al., 1999), most of which were, however, performed at very low spectral resolutions (typically from ~ 0.1 to 4 cm^{-1}) at room temperatures. The experimental study of Khlifi et al. (1992) covered a broad temperature range (219–328 K), but their unexpectedly strong temperature dependence of integrated band intensities (up to 21%) caught attention, prompting further investigation. Later, Rinsland et al. (2008) provided cross sections of benzene in a mixture of N_2 at 1 bar at three different temperatures (278, 298, and 323 K), showing no significant temperature dependence for the integrated band intensities. Moreover, substantial discrepancies were seen in the ν_4 band intensity between Khlifi et al. (1992) and Rinsland et al. (2008). It has been argued that poor spectral resolution was an issue for the ν_4 band measurements in the earlier work (Khlifi et al., 1992; di Lonardo et al., 1999). In this work new high-resolution measurements of benzene spectroscopy are described covering the ν_4 band near 674 cm^{-1} at temperatures relevant to the actual atmospheric conditions of Titan, Jupiter, and Saturn.

2. Benzene spectroscopy

Benzene has a hexagonal ring structure with one hydrogen atom attached to each of the six carbon atoms (Kekulé, 1890). The perfect symmetry results in no permanent dipole moment. Thus, pure rotational transitions in the microwave are suppressed by the symmetry so that atmospheric remote sensing must rely on its very dense and complex infrared spectrum arising from dipole moments induced by the 20 fundamental vibrations listed in Table 1.

However, only four of them are infrared active, but numerous infrared active overtones, combinations and hot bands can arise, especially from the states below 1000 cm^{-1} . Among the fundamental bands, the ν_4 centered at 673.9732 cm^{-1} (Lindemayer et al., 1988) is by far the strongest. This is attributed to its unique vibrational mode with all H atoms bending in and out of the carbon ring plane in unison. This unusually strong band permitted the early detection of benzene in our Solar System (Kim et al., 1985; Bézard et al., 2001; Coustenis et al., 2003, 2010) and beyond (Cernicharo, et al., 2001).

Benzene is also unusual in that the ν_4 Q-branch lines are ~ 20 times stronger than the ν_4 P- or R-branch lines, or the lines of any other band. This requires a large range of benzene amounts (i.e., column density) to capture the entire P, Q, R branch features well in the laboratory spectra. Hence we used two cells: one is 2.07 cm in length in which the ν_4 Q-branch is not saturated, and the other 80 cm in length in which weaker benzene lines are easily observable.

Due to the low-frequency vibrational modes, benzene features in the 7–15 μm region are expected to be heavily overlapped by hot band contributions, amounting to $\sim 45\%$ at room temperature and $\sim 25\%$ at 235 K (estimated by the vibrational partition function based on a simple harmonic oscillator approximation). Due to its heavy molecular mass (78.11 amu) all of its bands are very compact (e.g., ν_{13} at 1486 cm^{-1} is only $\sim 40\text{ cm}^{-1}$ wide), so that its densely-populated spectral features make detailed line-by-line characterization very challenging from the laboratory measurements. Several attempts were made to construct Hamiltonian models for the benzene transitions, but all of them studied only cold bands (Pliva and Johns, 1983, 1984; Pliva et al., 1989, 1991, 1993). The HITRAN database (Rothman et al., 2009, 2013) contains no line-by-line parameters for benzene (C_6H_6), while the GEISA 2009 database (Jacquinet-Husson et al., 2011) includes 8983 benzene transitions in the 642–705 cm^{-1} region. It is suggested by Rinsland et al. (2008), however, that the overall ν_4 band intensity listed in the GEISA 2009 database need to be reanalyzed.

Detailed characterization of the benzene spectral features is critical for planetary atmospheric observations, especially at 650–730 cm^{-1} (15 μm), where many other molecular features overlap; these include, e.g. on Titan, C_2H_2 at 730 cm^{-1} , CO_2 at 667 cm^{-1} , C_2HD at 678 cm^{-1} , and HC_3N at 663.0 cm^{-1} and 658.7 cm^{-1} (Coustenis et al., 2003, 2008, 2010; Jennings et al., 2008). To provide more realistic laboratory input for the spectroscopic observations of the Titan and Jovian atmospheres, we measured temperature dependent cross sections of benzene. For this, we employed high spectral resolution capturing the detailed structure in the

Table 1
Band centers of benzene ($^{12}\text{C}_6\text{H}_6$) fundamentals^a.

ν_n^b Herzberg	Band centers (cm^{-1})	Vib. sym.	dgn ^c	ν_n Herzberg	Band centers (cm^{-1})	Vib. sym.	dgn ^e
ν_1	3073.942	a_{1g}	1	ν_{11}	847.1062	e_{1g}	2
ν_2	993.071	a_{1g}	1	ν_{12}	3047.908^d	e_{1u}	2
ν_3	1350	a_{2g}	1	ν_{13}	1483.985^d	e_{1u}	2
ν_4	673.97465^d	a_{2u}	1	ν_{14}	1038.267^d	e_{1u}	2
ν_5	3057	b_{1u}	1	ν_{15}	3057.04	e_{2g}	2
ν_6	1013.74	b_{2u}	1	ν_{16}	1609.518	e_{2g}	2
ν_7	992.93	b_{2g}	1	ν_{17}	1177.776	e_{2g}	2
ν_8	702.24	b_{2u}	1	ν_{18}	608.13	e_{2g}	2
ν_9	1309.4	b_{2u}	1	ν_{19}	967.98	e_{2u}	2
ν_{10}	1147.6751	b_{2u}	1	ν_{20}	398.131	e_{2u}	2

^a Band centers adopted from NIST Chem Web (<http://webbook.nist.gov/chemistry>), VPLwebsite (<http://vpl.astro.washington.edu/spectra/fundamentals.htm>), Cané et al. (1997), and Miani et al. (2000).

^b Band labels are in Herzberg system (Herzberg, 1968).

^c dgn is for the vibrational degeneracy.

^d IR-active.

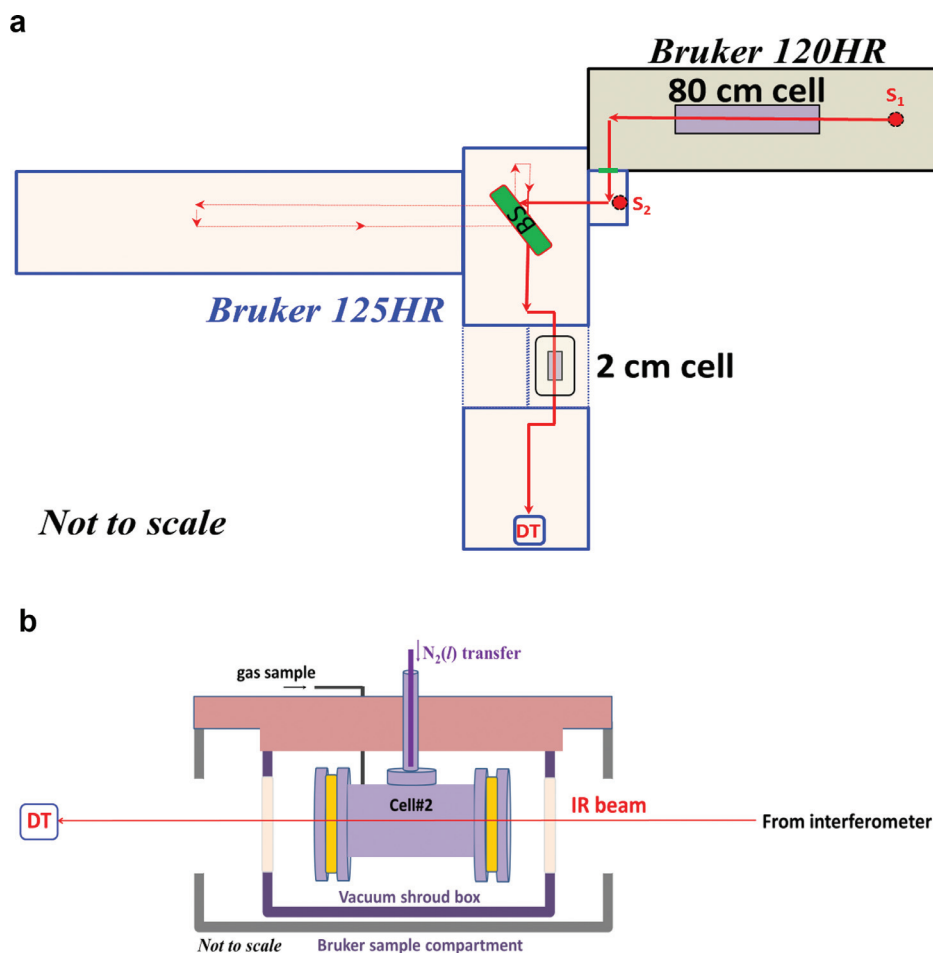


Fig. 1. (a) Simplified schematic diagram of Bruker IFS-125HR with the vacuum extension chamber configured through the emission port of the Bruker IFS-125HR. It shows the positioning of the 80 cm and 2.07 cm long cells; The 80 cm long cell was placed in front of the interferometer using the external source, S_1 , while the 2.07 cm long short cell was placed behind the interferometer using the internal source, S_2 . (b) Schematic diagram of the 2.07 cm long stainless cell housed in its own separate vacuum shroud box inside the sample compartment of the Bruker 125HR.

absorption features. Our measurements also covered a wide temperature range (298–235 K), the coldest temperature being limited by the benzene vapor pressure. The contributions from unidentified combination, overtone and hot bands are included in the analysis. We derived the cross sections and integrated band intensities of benzene (C_6H_6) in the ν_4 at 673, ν_{14} at 1038, and ν_{13} at 1468 cm^{-1} from N_2 -broadened spectra combined with high resolution pure benzene spectra for Titan atmosphere. We also measured the benzene cross sections from (85% H_2 + 15%He) mixture-broadened spectra for the study of Jovian atmospheres.

Finally, we have taken an additional step to make our results more amenable to line-by-line calculations. As was discussed in the experimental study of propane (C_3H_8) (Sung et al., 2013), we have generated a benzene *pseudo-linelist* (PLL) compiled in the HITRAN-format (Rothman et al., 2013), from which benzene cross sections or opacity can be computed at any temperature or pressure. While this PLL is most accurate when used within the range of T/P used in the laboratory measurements, it can also be used to extrapolate in T/P. We estimate uncertainties of up to $\sim 30\%$ when the PLL is used for extreme temperatures down to 100 K. This empirical PLL approach therefore provides an effective alternative to true spectroscopic line parameters in radiative transfer calculations until a full line-by-line quantum mechanical analysis becomes available. Finally, we present the PLL files for benzene as electronic supplements.

3. Experimental details

A total of 34 sets of high-resolution absorption spectra of benzene were recorded at temperatures between 235 K and 297 K using two cold cells (80 cm and 2.07 cm path long, respectively) coupled to a Bruker IFS-125HR Fourier-transform infrared (FT-IR) spectrometer at the Jet Propulsion Laboratory (JPL). The spectrum sets include 15 pure and 15 N_2 -broadened spectra in the $630\text{--}1534\text{ cm}^{-1}$ region, and four additional spectra broadened by a pre-mixture gas of H_2 (85%) and He (15%) in the $630\text{--}740\text{ cm}^{-1}$ region.

The 80 cm long straight-pass cold cell, originally developed and used at Kitt Peak Obs., AZ (Margolis et al., 1990), was made of stainless steel with copper tubes silver-soldered around the cell body for cooling gas flow, which was constantly supplied by a liquid N_2 tank and then passing through a copper coil in a large open-mouth N_2 dewar. The temperature of the cell was monitored using three sets of Type T thermocouples attached to the cell body, with the reference end dipped into ice water for zero-point calibration. The entire cell system (the cell and cooling tubes) was placed inside a vacuum extension chamber adapted from a retired Bruker IFS-120HR (See Fig. 1a). A separate external light source (Globar) was installed in the vacuum extension chamber along with proper optics (e.g., an off-axis parabola mirror) to collimate the infrared beam, which passed through the 80 cm long cell and then into the Bruker 125HR interferometer through its emission port. Since the

external source and the transfer optics are movable, this arrangement permitted any gas absorption cell shorter than 1.5 m long to be used for other experiments with same the Bruker 125HR (e.g., Drouin et al., 2013). The extension chamber remained evacuated to ~ 30 mTorr during the entire scanning.

The short 2.07 cm cold cell was placed inside the sample compartment of the Bruker IFS-125HR (See Fig. 1b). As described in Varanasi and Chudamani (1989) (who developed the cell at Stony Brook University), the cell refrigeration system has a unique three-layered LN₂ transfer system consisting of vacuum jacket (outermost), cold N₂ gas return line (middle), and LN₂ supply line (innermost) for the cryotip. While in use, the cold cell was attached to the cryotip of the LN₂ supply line. A pair of indium-sealed ZnSe windows was installed to the cell. Replacement of the O-ring re-assembly during the experiment produced slightly different absorption path lengths for the short-path cell (2.07(5) and 2.06(4) cm, respectively) measured after each re-assembly. The uncertainty, mostly due to squeezing the O-ring, was judged to be significant and is a primary source of absolute accuracy for the cross sections. The short cell was shrouded in its own separate vacuum box sealed with KBr windows to protect the cold ZnSe windows from cryodeposits. Two sets of Si–Di temperature sensors were attached to the cell body; one on the top near the cold finger, and the other on the side. The latter one was used to monitor the cell temperature.

Temperature uniformity across the short cell was maintained at better than 1.5 K during scanning. The temperature of the cold cells was regulated by adjusting the cold gas flow with no heater for the 80 cm long cell and with a heater for the 2.07 cm long cell. Because small temperature drifts/fluctuations (~ 2.5 K) and temperature gradient (~ 1.5 K) across the cells were seen during the scanning, the measurement temperature uncertainties for the cold spectra were estimated to be ~ 2.9 K. The measurement temperature range adopted in this work was limited by the available benzene vapor pressure. As shown in Fig. 2, the benzene vapor pressures rapidly drop at lower temperatures (Lide DR, 1998, 2011; Poltoratskii, 1962 (cited in <http://www.ddbst.com>); ChERIC, 2015 (CHERIC fit, <http://www.cheric.org>). Only a fraction of the estimated saturated vapor pressure was used in the experiment to avoid possible condensation of the benzene sample inside the cell.

An anhydrous high-purity (99.98%) sample of benzene (with no isotope-enrichment) was purchased from Sigma-Aldrich, Inc., so the reported benzene cross sections do not discriminate contributions from its four most abundant minor isotopologues; based on the PDB values for ¹³C/¹²C and D/H, the relative abundance in percent are computed to be 93.48, 6.27, 0.18, and 0.06% for ¹²C₆H₆, ¹³C ¹²C₅H₆, ¹²C₄¹³C₂H₆, and ¹²C₆H₅D, respectively. We note that our value for ¹²C₆H₆ is in good agreement with the value, 93.43%, quoted by Dang-Nhu and Pliva (1989). The liquid benzene sample was held in a light-shielded glass tube and purified by using a freeze-and-thaw procedure several times, then used with no further purification. Residual H₂O features were seen, particularly in

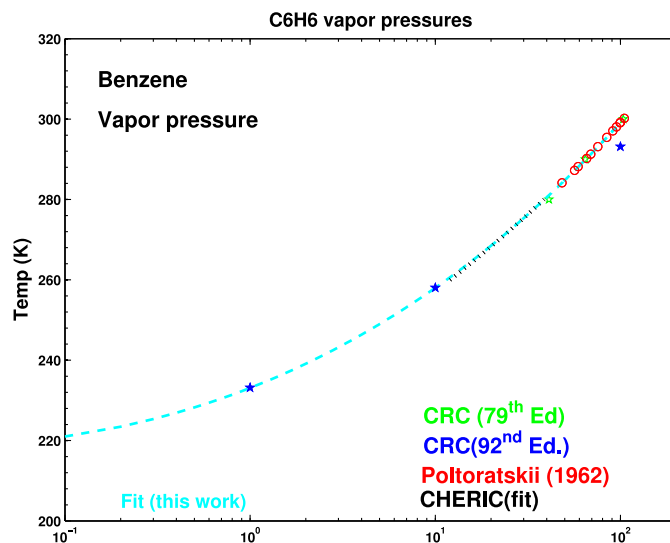


Fig. 2. Saturation vapor pressure of benzene adopted in this work from CRC, 79th and 92nd ed., Poltoratskii (1962), ChERIC (<http://www.cheric.org>).

the spectra at room temperatures, but these were removed spectroscopically while generating benzene pseudolines (see Section 6). Other hydrocarbon residues are reported to be a few ppm, but no attempt was made to identify them in this work. The liquid benzene was let to evaporate at room temperature and guided into each cell, followed by insertion of either research grade N₂ gas (99.9999%) or high purity pre-mixture of 85% H₂ + 15% He for pressure-broadened spectra. Sample pressures were continuously monitored using Baratron pressure gauges. Prior to cooling, the absorption cell was pumped for several hours to remove all residual gases, including water vapor degassing from the cell walls.

As summarized in Table 2, the instrumental set-up was configured with a Globar infrared light sources (an external Globar S₁ for the 80 cm long cell and an internal Globar source S₂ for the 2.07 cm long cell as illustrated in Fig. 1a), a KBr beam splitter, and liquid N₂-cooled MCT detector. The interferometer was set up with various maximum optical path differences (MOPD) between 50 and 225 cm, providing unapodized spectral resolution from 0.0022 and 0.044 cm⁻¹. An optical filter provided the desired band pass of 620–1550 cm⁻¹ when combined with the MCT detector response. The entire optical beam path was evacuated to a pressure of ~ 10 mTorr during the experiment, which minimized interferences from residual water vapor in the Bruker FT-IR chamber. A summary of the experimental conditions for the cold spectra is provided in Table 3. Since Doppler-limited spectral resolution for benzene (0.001 cm⁻¹) is hard to achieve with our FT-IR, we selected basically several different spectral resolutions (0.0022–0.044 cm⁻¹) adaptively to the sample pressures and temperatures considering

Table 2
Instrumental configuration for the benzene scanning.

Samples	Anhydrous C ₆ H ₆ (99.8%)	N ₂ (99.9999%), and	H ₂ (85%) + He(15%)
Run names	B0108 series	B0111, B0123 series	B0123 series
Spectral region	7–15 μm (630–1535 cm ⁻¹)	15 μm (630–730 cm ⁻¹)	15 μm (630–730 cm ⁻¹)
Bands	v ₄ , v ₁₄ , v ₁₃ , v ₁₇ +v ₂₀ , etc.	v ₄ and its hot bands	v ₄ and its hot bands
Path lengths	80 cm	2.07 cm	2.06 cm ^a
Detectors	HgCdTe	HgCdTe	HgCdTe
Temperatures	235–296 K	242–297 K	235–260 K
Pressures	P _s : 0.018–5.2 Torr P _{tot} : 0.452–596.2 Torr	P _s : 0.578–1.352 Torr P _{tot} : 0.578–297.6 Torr	P _s : 0.54–2.43 Torr P _{tot} : 0.54–225.3 Torr
# of spectra	17	13	4

^a Measured after re-assembling.

Table 3
Experimental conditions of the N₂- and (H₂+He) mixture-broadened C₆H₆ spectra.

Spectra	Temp	P _t (Torr)	P _s (Torr)	Resolution	Calibration factors
Pure C ₆ H ₆	650–1550 cm ⁻¹ region with 80 cm cell				
B0108.2a	296.2	0.774	0.774	0.01	1.000001856850
B0108.2c	296.2	5.250	5.250	0.01	1.000001840753
B0108.5a	273.3	3.874	3.874	0.01	1.000001827028
B0108.1d	259.0	0.614	0.614	0.01	1.000001911800
B0108.4a	252.3	0.780	0.780	0.01	1.000001806949
B0108.3b	245.2	0.452	0.452	0.01	1.000001976156
Pure C ₆ H ₆	650–690 cm ⁻¹ region with 2 cm cell				
B0111.2a	297.3	0.764	0.764	0.005	1.000000437878
B0111.1a	296.8	1.354	1.354	0.0056	1.000001034423
B0111.1e	296.7	0.925	0.925	0.005	1.000001027227
B0111.1b	296.0	0.810	0.810	0.0022	1.000000998757
B0123.2d	263.3	0.54	0.54	0.0022	1.000000425628
B0123.2a	258.7	2.430	2.430	0.0033	1.000000436323
B0111.2b	252.6	0.578	0.578	0.005	1.000000450546
B0111.4a	242.0	0.642	0.642	0.005	1.000000450542
B0123.3a	236.3	0.590	0.590	0.0022	1.000000447238
C ₆ H ₆ +N ₂	650–1550 cm ⁻¹ region with both cells				
B0111.3e	297.9	149.5	1.030	0.01	1.000000436677
B0108.2d	296.2	211.8	5.250	0.01	1.000001868717
B0108.2e	296.2	77.84	1.929	0.01	1.000001880727
B0111.1c	296.0	212.1	0.844	0.01	1.000001028393
B0108.2b	295.8	167.5	0.774	0.01	1.000001861655
B0108.5b	273.3	282.9	3.874	0.01	1.000001838641
B0111.2d	260.3	297.6	0.5968	0.044	1.000000570286
B0108.1b	259.0	79.75	0.614	0.01	1.000001878668
B0108.1c	258.5	111.3	2.315	0.01	1.000001883999
B0108.6h	255.1	596.2	0.047	0.04	1.000001552289
B0108.4b	252.5	126.6	0.780	0.01	1.000001897249
B0108.3c	245.0	339.8	0.452	0.01	1.000001837477
B0108.3a	243.0	79.03	0.076	0.01	1.000001805334
B0108.6f	235.3	458.9	0.018	0.02	1.000001894586
B0123.4a	235.2	95.19	0.610	0.005	1.000000451902
C ₆ H ₆ +H ₂ +He	630–690 cm ⁻¹ region with 2 cm cell				
B0123.1c	296.7	225.3	2.005	0.005	1.000000410499
B0123.1d	296.8	89.63	0.798	0.0033	1.000000411886
B0123.2b	261.6	213.5	2.430	0.0066	1.000000420621
B0123.3b	236.0	175.2	0.590	0.005	1.000000441735

combined Doppler and Lorentz widths. Empty cell spectra were taken at spectral resolutions matching their gas sample spectrum counterparts, facilitating point-by-point ratioing to obtain transmittance spectra. The individual spectra were selectively coadded after inspecting them for any possible baseline degradation due to ice absorption features. Finally a S/N of ~150:1 was achieved for the transmittance spectra analyzed in this work.

The frequency calibration factors were determined from all unratiod spectra since water vapor features arising from the Bruker 125HR chamber were mostly removed in the ratioing. Line center positions of water in the ν_2 and $2\nu_2-\nu_2$ bands in the 1390–1550 cm⁻¹ region observed in the individual unratiod spectra were compared to the HITRAN 2012 database (Rothman et al., 2013) to derive the frequency calibration factors listed in Table 3, which were applied to their corresponding ratioed (i.e., transmittance) spectra analyzed in this work. The resultant overall frequency precision was measured to be better than 5×10^{-4} cm⁻¹ after the calibration.

4. Measured transmittance spectra of benzene

Examples of transmittance spectra from 630 cm⁻¹ to 1530 cm⁻¹ are shown in Fig. 3 using pure and N₂-broadened C₆H₆ recorded at 296 and 255 K. The individual observed bands are ν_4 at 673.973 cm⁻¹, $\nu_{17}-\nu_{20}$ at 779.6 cm⁻¹, ν_{14} at 1038.267 cm⁻¹, $\nu_7+\nu_{20}$ at 1388 cm⁻¹, and ν_{13} at 1483.985 cm⁻¹ with some contribution from $\nu_4+\nu_{11}$ at 1522 cm⁻¹. Other weaker features from $\nu_2+\nu_{18}-\nu_{20}$ at 1212, $\nu_{11}+\nu_{20}$ at 1242 cm⁻¹ were also identified, but their

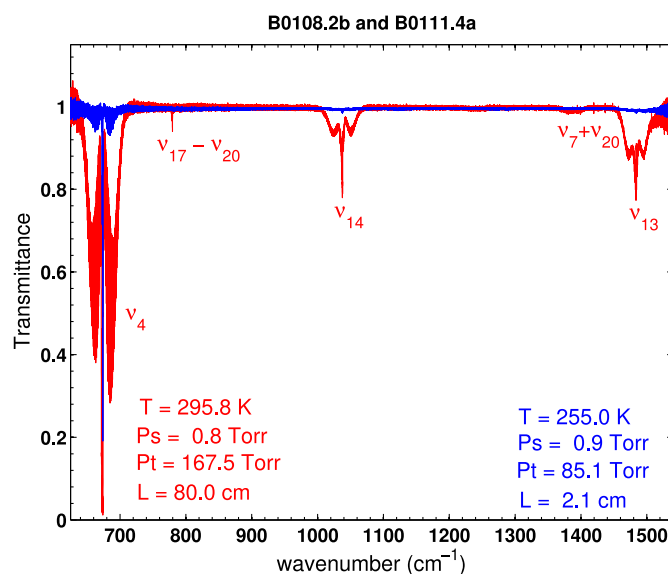


Fig. 3. N₂-broadened spectra of C₆H₆ at 295.8 (in red) and 255 K (in blue), showing relative band strengths for five distinctive bands including the ν_4 , ν_{14} , and ν_{13} fundamentals at 674, 1038, and 1425 cm⁻¹, respectively.

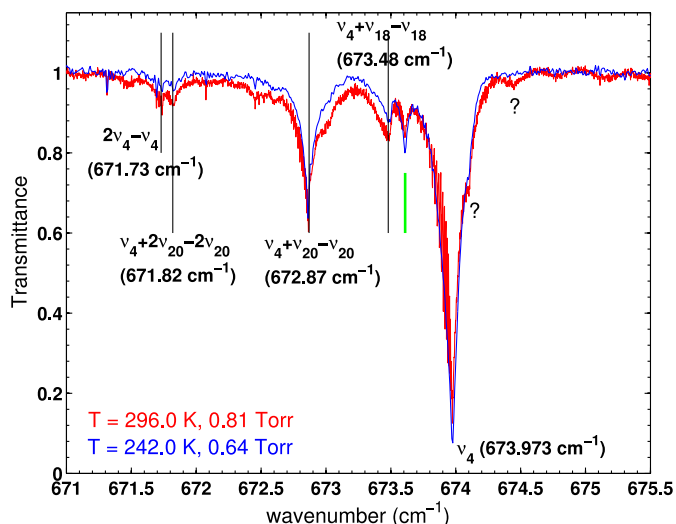


Fig. 4. Four $^{12}\text{C}_6\text{H}_6$ hot bands and one $^{13}\text{C}^{12}\text{C}_5\text{H}_6$ feature (in green) were observed near the band centers reported by Snaveley et al. (1984). Two more features (labeled as ?) in the region were seen, but yet to be identified. See text for details.

cross sections are not reported in this work. Distinct Q branches near the band center are easily seen for some bands. There are many line-like features even in the pressure-broadened spectra each band, which are the non-zero J family of Q_J sub-branches. It should be recalled that, for the H_2+He pre-mixture-broadened benzene, their spectra were recorded only in the $630\text{--}690\text{ cm}^{-1}$ region and analyzed mainly for the strongest ν_4 band.

As expected, some hot bands were observed in the ν_4 band region, as shown in Fig. 4. The features at 671.736 , 671.825 , 672.866 , 673.487 cm^{-1} correspond within 0.01 cm^{-1} to the $2\nu_4-\nu_4$, $\nu_4+2\nu_{20}-\nu_{20}$, $\nu_4+\nu_{20}-\nu_{20}$, and $\nu_4+\nu_{18}-\nu_{18}$ bands of $^{12}\text{C}_6\text{H}_6$ reported by Snaveley et al. (1984) (at 671.73 , 671.82 , 672.87 , 673.48 cm^{-1} , respectively). However, the feature at 673.609 cm^{-1} (marked by green vertical line) appears to be the ν_4 Q -branch of $^{13}\text{C}^{12}\text{C}_5\text{H}_6$, whose frequency offset from that of main isotopologue $^{12}\text{C}_6\text{H}_6$ was observed to be 0.364 cm^{-1} , consistent with the value (0.37 cm^{-1}) reported by Snaveley et al. (1984). It is also obvious from Fig. 4 that the absorption peak at 673.609 cm^{-1} belongs to a cold band because it strengthened at the colder temperature, despite the lower sample pressure. Two more features (marked as ?) were observed at 674.101 and 674.448 cm^{-1} , but not identified.

We have analyzed the transmission spectra by splitting into six well-isolated regions (five regions for the pure and N_2 -broadened spectra and only region of the ν_4 region for (H_2+He)-broadened spectra), which are detailed in Table 4. Out of the total 34 measured spectra obtained at the various temperatures and pressures listed in Table 3, a different combination of pure and pressure-broadened spectra was selected for each Region based on their optical depths and signal-to-noise. For instance, the Q -branch near

674 cm^{-1} in the Regions I and VI was observed to be saturated in almost all the spectra recorded with the 80 cm long cell, while those features showed useful absorption depths in the spectra from the 2.07 cm long cell. As a result, all the spectra were analyzed for the ν_4 band. However, the $\nu_{17}-\nu_{20}$ band in Region II was barely observable in the spectra from the short cell, so only a limited set of spectra were selected and analyzed.

5. Calculation of cross-sections

Measuring individual C_6H_6 transitions line-by-line is extremely challenging even at low sample pressures, and with Doppler-limited resolution. The process is further complicated by numerous overlapping weak features arising from hot- and combination/overtone-bands. As seen in Figs. 3–5, for the pure samples at low pressure (Fig. 5a), the J and K manifold structures are not resolved. In the N_2 -broadened spectra (Fig. 5b) the transitions blend to produce broad unresolvable continua. To provide essential information needed for atmospheric remote sensing, we therefore measured benzene cross sections, $\kappa_{\text{obs}}(\nu)$ in $\text{cm}^2/\text{molecule}$, directly calculated from the observed transmittance spectra, $\tau_{\text{obs}}(\nu)$, by $\kappa_{\text{obs}}(\nu) = -\ln[\tau_{\text{obs}}(\nu)]/(n\xi l)$, where n , ξ , and l are number density ($\#/\text{cm}^3$), mixing ratio, and absorption path length (cm), for the six Regions listed in Table 4. It is noted that intensities of other absorption features outside the specified spectral regions are insignificant, so they were not included in the analysis.

Examples of the measured cross sections are presented in Fig. 5. Their respective pure sample pressure and total mixture pressures are labeled on the figures along with the measurement temperatures. In Fig. 5a and b, pure and N_2 -broadened spectra of benzene in the ν_4 region are compared to show the substantial pressure broadening for the N_2 -broadened spectra at both conditions. All the line-like features in the P and R branches of the band are, in fact, J -manifolds with many K sub-bands. Since their apparent widths are much broader than that of an isolated single C_6H_6 transition, an instrumental spectral resolution larger than the Doppler limit was acceptable for the data acquisition without significant loss of information. Also, it is worthwhile to note that the strengths of the lower J -manifolds are significantly enhanced at the colder temperature, resulting in the band width seemingly narrowed when compared to the data at warm temperature. As a result, such intensity redistribution at cold temperatures is expected to produce more outstanding features for the Q branch of the cold band at 674 cm^{-1} , but diminish the absorption peak for the hot band Q -branch at 672.4 cm^{-1} . The cross sections presented in Fig. 5c the ν_{14} region and Fig. 5d the ν_{13} region at 295.8 and 245 K also show a similar intensity enhancement of lower J -manifolds for the cold band.

It should be recalled that, since these are direct measurements of the absorption features, the cross sections at a given frequency include all contributions from unidentified combination and hot

Table 4
List of spectral regions separately discussed in this work^a.

Regions	Range (cm^{-1})	Bands observed	No. of spectra	No. of spectra
Region I	630–735	ν_4	15 pure C_6H_6	15 ($\text{C}_6\text{H}_6 + \text{N}_2$)
Region II	740–840	$\nu_{17}-\nu_{20}$	6 pure C_6H_6	8 ($\text{C}_6\text{H}_6 + \text{N}_2$)
Region III	950–1100	ν_{14}	11 pure C_6H_6	11 ($\text{C}_6\text{H}_6 + \text{N}_2$)
Region IV	1340–1425	$\nu_7 + \nu_{20}$	9 pure C_6H_6	11 ($\text{C}_6\text{H}_6 + \text{N}_2$)
Region V	1425–1538	ν_{13} , $\nu_4 + \nu_{11}$	3 pure C_6H_6	7 ($\text{C}_6\text{H}_6 + \text{N}_2$)
Region VI	630–735	ν_4	15 pure C_6H_6	4 ($\text{C}_6\text{H}_6 + \text{H}_2 + \text{He}$) ^b

^a Measured cross sections in this work include contributions from minor isotopologues of benzene.

^b Pre-mixture sample of $\text{H}_2(85\%)$ and $\text{He}(15\%)$ was used.

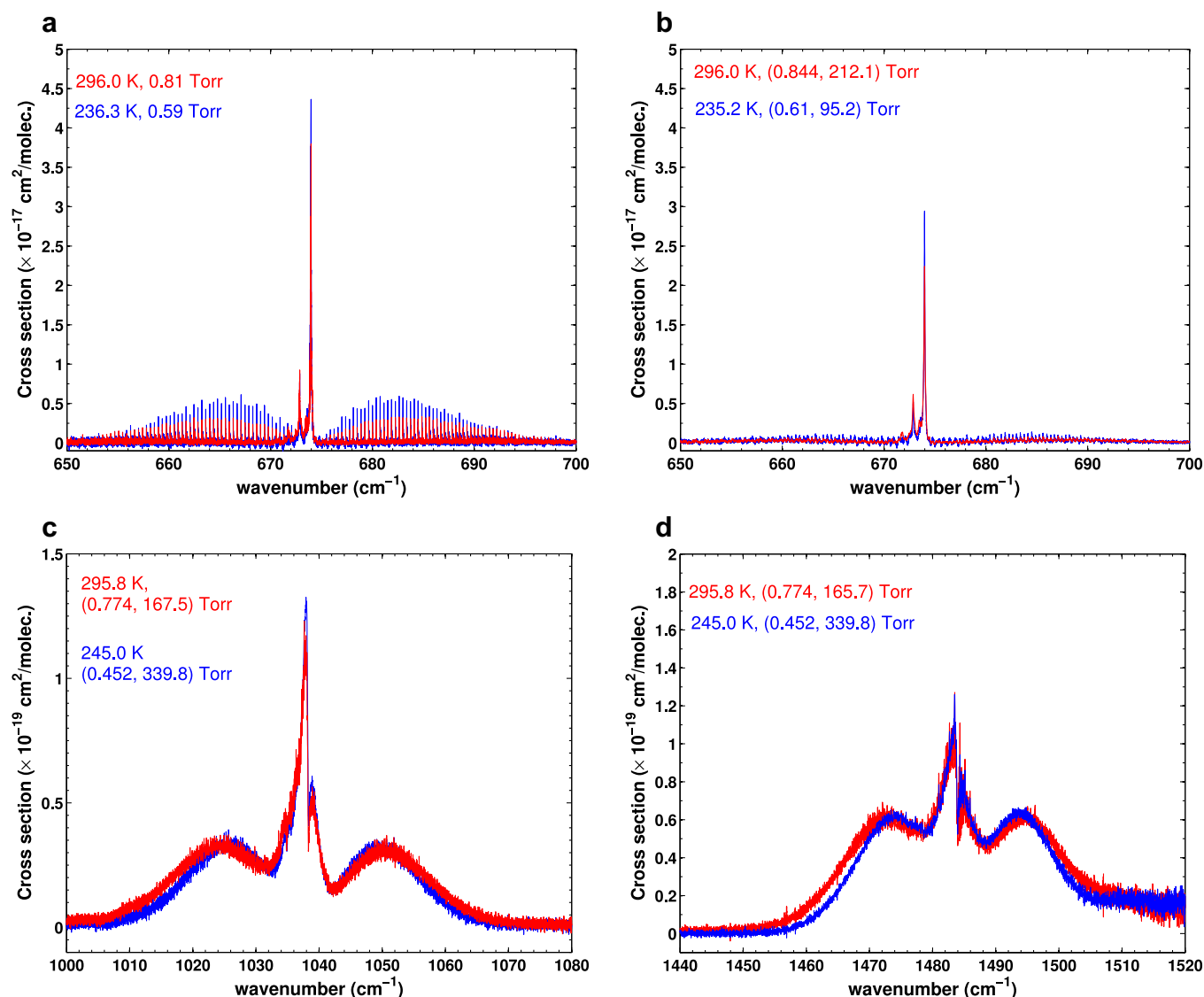


Fig. 5. Cross sections of benzene. Region I. (a) pure and (b) N_2 -broadened; (c) and (d) show N_2 -broadened results for Regions III and V derived from spectra measured with the same cell.

bands, as well as the fundamental cold bands specified in Tables 1 and 4. We note that band intensity, S_V $cm^{-1}/(molecule \cdot cm^{-2})$, is considered as one of the most useful fundamental spectroscopic properties, providing insight on molecular structure and band-to-band interactions as well as a practical guideline for applications in atmospheric remote sensing. An integrated band intensity, A_B in $cm^{-1}/(molecule \cdot cm^{-2})$, can be obtained by summing up all line intensities over the spectral region and also can be written (Dang-Nhu et al., 1989) using the band intensity, S_V :

$$A_B(T) \approx S_V \times Q_{vib}(T) \quad (1)$$

where Q_{vib} is vibrational partition function at temperature T . It is well known that, for isolated fundamental bands, their band intensity is independent of temperature (Crawford Jr. et al., 1958; Breeze et al., 1965). Meanwhile, an integrated cross section, X_B in $cm^{-1}/(molecule \cdot cm^{-2})$, is computed by summing up the measured cross sections over the range of wavenumbers for a band. However, as discussed in Sung et al. (2013), the integrated cross section, X_B , for a particular band is not necessarily equal to the integrated band intensity, A_B , because all the absorption features in the observed spectrum may not be fully resolved at the spectral resolution of the measurements. This is particularly expected for heavy

molecules in the mid-infrared region where Doppler widths are very small, beyond the instrumental resolutions available. Therefore, we have estimated integrated band intensity, A_B , by summing up individual line intensity parameters of ‘pseudolines’, as discussed below.

6. Pseudoline generation

In this work, in addition to calculating cross sections from individual transmittance spectra described in Section 5, we have also adopted the empirical pseudoline generation approach to develop a HITRAN-like PLL for benzene in the 7–15 μm region. Briefly summarizing, over a narrow wavenumber interval the mean absorption coefficient may be modeled by a set of ‘effective’ line parameters (line intensity S and lower state energy E'') derived from laboratory spectra. A physically-based model for the pseudoline approach was introduced by Toon et al. (1992, 1999) by assuming that valid average transmission can be defined for a given frequency grid, *i.e.*, typically uniformly-spaced frequency bins treated as pseudolines. The pseudolines are compiled as ‘individual transitions’, *i.e.*, assuming that they have valid mean values of line position, strength, pressure-broadened widths,

Table 5

List of all the assumed parameters fixed in the pseudoline generation.

Parameters	Values	References
Frequency grid spacing	0.005 cm ⁻¹	See text
Modified Doppler full width (fixed)	0.005 cm ⁻¹	See text
Self-broadened half width at 296 K	0.18 cm ⁻¹ /atm	Waschull et al.(1998)
N ₂ -broadened half width at 296 K	0.12 cm ⁻¹ /atm	Waschull et al.(1998)
N ₂ -broadened half width at 296 K near 674 cm ⁻¹	0.24 cm ⁻¹ /atm	Assumed; See text
(H ₂ +He)-broadened half width at 296 K	0.163 cm ⁻¹ /atm	Assumed; See text
T-dependence for pressure-broadened width	0.75	Assumed; See text
Pressure-induced frequency shift	-0.003 cm ⁻¹ /atm	Assumed

and lower state energy, E'' . This approach was successfully implemented for atmospheric spectroscopic observations (Toon et al., 1992, 1999), and for laboratory spectrum analysis (Sung et al., 2013). Further details can be found on-line (<http://mark4sun.jpl.nasa.gov/data/spec/Pseudo/Readme>). Among many advantages expected for this PLL approach for polyatomic molecules, are the following; (1) one single line list can be used to accurately reproduce the cross sections measured at any temperatures and pressures encompassed by the laboratory measurements from which the PLL was derived, (2) since the pseudolines were derived via fitting multiple spectra by adopting a physical line shape model and instrumental line shape function, the pseudoline parameters are instrument- and resolution-independent. Therefore, they can be used with any existing line-by-line calculation models as an effective spectroscopic input, and (3) spectral features from any known impurities (e.g., water vapor transitions) can be modeled during the spectral fitting, so that the derived pseudolines are impurity-free. This is especially important for molecules whose features show up in the vicinity of the strong water bands, like those for benzene in the ν_{13} region (Region V). Furthermore, the pseudoline intensities allow a more estimate of the integrated band intensity than integrating the measured cross sections (X_B) because the pseudoline intensities are determined based on a physical line profile model (e.g., Voigt line shape profile, the widely accepted empirical law of the pressure broadening) and realistic partition functions, resulting in lower sensitivity to the experimental conditions (such as pressures and temperatures).

From the 30 pure and N₂-broadened benzene spectra recorded covering 235–297 K, we have derived a 296 K intensity S , and an empirical lower state energy E'' for all the individual ‘pseudolines’. The line spacing for the pseudolines was chosen to be 0.005 cm⁻¹ by trading off retrieval precision and computation cost in the line-by-line calculations. For the physical model of molecular line shape, we adopted Voigt line shape profile to compute a spectrum at sufficiently high resolution (e.g., 0.001 cm⁻¹), which then is convolved with instrumental line shape function (ILS). For the ILS, we used *sinc* function convolved with the field of view function (see Booth et al., 1985). However, the Doppler width has been set to be the same as equidistance spacing, 0.005 cm⁻¹, in this work, and held fixed for all temperatures. Pressure-broadening of individual transitions was accounted for by taking the pressure-broadened half-width coefficients with temperature dependences in an analogy to the true spectroscopic line parameters. Waschull et al. (1995, 1997, 1998) reported self- and N₂-broadened half widths of benzene up to $J=66$, showing no distinctive dependence on rotational quantum numbers, J and K . They measured self-broadened widths to be 0.12–0.22 cm⁻¹/atm at 296 K and their temperature dependence exponent, n , defined by Eq. (2), to be 0.47 in the range of warm temperatures, 296–344 K.

$$b(T) = b(T_0) \times \left(\frac{T_0}{T}\right)^n \quad (2)$$

For N₂-pressure broadened width, three Q-branch transitions of ν_{14} (belong to Region III listed in Table 3) were reported to be

0.086, 0.117, 0.119 cm⁻¹/atm at 296 K, from which 0.12 cm⁻¹/atm at 296 K has been suggested for both air and N₂-broadened width as a representative value. Therefore, we adopted 0.18 and 0.12 cm⁻¹/atm at 296 K for self and N₂-broadened widths of benzene, respectively, for all the pseudolines. However, for the ν_4 Q-branch region near 674 cm⁻¹, we adopted the self-broadened width of 0.24 cm⁻¹/atm at 296 K, since we found that the increased width produced significantly better spectral fitting residuals. Temperature dependence exponents have been assumed to be $n=0.75$ for both N₂- and self-broadening by adopting a theoretical value (Anderson et al., 1949) instead of using the value derived from the measurements of Waschull et al. (1998) at warm temperatures.

The pseudolines are a set of empirical parameters as a mathematical construct over the assumed frequency bins to represent absorption features. The pseudoline intensity and lower state energy parameters are closely coupled to the choice of other line parameters such as pressure-broadening coefficients. Since a different set of pressured-broadened widths was required for the H₂+He-broadened benzene spectra, a separate pseudoline list was generated. For the H₂+He-mixture broadening of benzene, however, we have adopted the half-width to be 0.163 cm⁻¹/atm at 296 K by combining (1) measurements of He-broadened width (0.11 cm⁻¹/atm) of benzene in the ν_{14} band (Waschull et al., 1998), (2) borrowing the ratio (i.e., 1.565) of H₂- to He-broadened width for another polyatomic hydrocarbon, ethane (C₂H₆) (Blass et al., 1987), and then (3) applied the estimated values proportionately to the mixture of H₂(85%) and He(15%). All the assumed parameters in the pseudoline generation are summarized in Table 5.

All the spectra were fit simultaneously to derive line strengths (S) at 296 K and lower state energies (E'') of the individual pseudolines by

$$\frac{S(T)}{S(T_0)} = \frac{Q_{vib}(T_0) Q_{rot}(T_0)}{Q_{vib}(T) Q_{rot}(T)} \times e^{-C_2 E''(1/T - 1/T_0)} \times \left(\frac{1 - e^{-C_2 \nu_j/T}}{1 - e^{-C_2 \nu_j/T_0}} \right) \quad (3)$$

where $S(T_0)$ is the line strength (cm⁻¹/(molecule·cm⁻²)) at the reference temperature $T_0=296$ K, the last term in the parenthesis is for the stimulated emission, ν_j being the pseudoline frequency (cm⁻¹). The term $\exp[-C_2 E''(1/T-1/T_0)]$ is the Boltzmann factor, the second Boltzmann constant $C_2=1.4388$ cm/K, E'' being the empirical lower state energy (cm⁻¹) of the individual pseudoline transitions. The vibrational partition function, Q_{vib} , at a given temperature T was computed using harmonic oscillator approximation by,

$$Q_{vib}(T) = \prod \left(\frac{1}{1 - e^{-C_2 E_{v,n}/T}} \right)^{dgn} \quad (4)$$

where, E_v is vibrational energy level (band center), n is an index of normal modes ($n=1-20$), dgn for degeneracy for each fundamental, all of which are listed in Table 1. Ratio of the rotational partition function Q_R at two different temperatures is approximated by $Q_R(T)/Q_R(T_0)=(T/T_0)^\beta$, where $\beta=1.5$ for non-linear molecule with no torsional band. In the iterative spectrum fitting, by combining

Table 6

An excerpt of the compiled pseudoline sample list for N₂-broadened benzene in the HITRAN 2000 format.

MMI	freq(cm ⁻¹)	S(296K)	N2–Self-	E''	n–shift–
730	674.040000	6.218E-20	0.000E+00.1200.2400	486.48290.75-.003000	
730	674.045000	2.691E-20	0.000E+00.1200.2400	386.07550.75-.003000	
730	674.050000	5.345E-20	0.000E+00.1200.2400	646.29670.75-.003000	
730	674.055000	3.135E-20	0.000E+00.1200.2400	557.81030.75-.003000	
730	674.060000	4.429E-20	0.000E+00.1200.2400	626.28320.75-.003000	
730	674.065000	3.158E-20	0.000E+00.1200.2400	536.63460.75-.003000	
730	674.070000	3.624E-20	0.000E+00.1200.2400	851.11390.75-.003000	
730	674.075000	3.121E-20	0.000E+00.1200.2400	567.57530.75-.003000	
730	674.080000	3.367E-20	0.000E+00.1200.2400	699.82110.75-.003000	
730	674.085000	3.280E-20	0.000E+00.1200.2400	662.51260.75-.003000	
730	674.090000	3.097E-20	0.000E+00.1200.2400	779.45760.75-.003000	
730	674.095000	3.096E-20	0.000E+00.1200.2400	862.93920.75-.003000	
730	674.100000	3.553E-20	0.000E+00.1200.2400	710.26090.75-.003000	
730	674.105000	3.275E-20	0.000E+00.1200.2400	839.79680.75-.003000	
730	674.110000	3.121E-20	0.000E+00.1200.2400	838.56400.75-.003000	
730	674.115000	2.278E-20	0.000E+00.1200.2400	910.72240.75-.003000	
730	674.120000	2.239E-20	0.000E+00.1200.2400	920.17200.75-.003000	
730	674.125000	2.285E-20	0.000E+00.1200.2400	875.79330.75-.003000	
730	674.130000	1.560E-20	0.000E+00.1200.2400	1054.60070.75-.003000	
730	674.135000	2.169E-20	0.000E+00.1200.2400	1078.95460.75-.003000	
730	674.140000	1.070E-20	0.000E+00.1200.2400	1272.96960.75-.003000	
730	674.145000	1.921E-20	0.000E+00.1200.2400	1339.72350.75-.003000	
730	674.150000	9.669E-21	0.000E+00.1200.2400	1279.80090.75-.003000	
730	674.155000	1.578E-20	0.000E+00.1200.2400	1660.88170.75-.003000	
730	674.160000	6.312E-21	0.000E+00.1200.2400	1744.14100.75-.003000	
730	674.165000	1.472E-20	0.000E+00.1200.2400	1696.04100.75-.003000	
730	674.170000	5.649E-21	0.000E+00.1200.2400	2000.69030.75-.003000	
730	674.175000	1.263E-20	0.000E+00.1200.2400	2415.31350.75-.003000	
730	674.180000	5.215E-21	0.000E+00.1200.2400	2653.02320.75-.003000	
730	674.185000	1.124E-20	0.000E+00.1200.2400	2408.74220.75-.003000	
730	674.190000	2.827E-21	0.000E+00.1200.2400	2373.38330.75-.003000	
730	674.195000	7.568E-21	0.000E+00.1200.2400	2267.63920.75-.003000	
730	674.200000	5.089E-21	0.000E+00.1200.2400	2635.96440.75-.003000	

Notes: MM= molecule index; l= isotopologue index. Set l=0 as an indicator of pseudoline line; wavenumber in cm⁻¹; line intensity, S, of benzene in natural abundance at 296K in cm⁻¹/(molecule.cm⁻²); N₂-broadened width, Self-broadened width in cm⁻¹/atm; E''=lower state energy (cm⁻¹); n = temperature dependence exponent for pressure broadened widths; Pressure-induced frequency shifts (cm⁻¹/atm). Note that the format for the first 67 columns each line is the same for all HITRAN database. Further details, See the HITRAN database (Rothman et al., 2009, 2013).

Eqs. (2)–(4), one can obtain Eq. (5) for a given *j*th spectrum,

$$\ln\left(\frac{\ln \tau_c}{\ln \tau_m}\right) \approx \ln \frac{S_c(T_0)}{S_m(T_0)} + C_2(E''_c - E''_m) \left(\frac{1}{T_0} - \frac{1}{T_j}\right) \quad (5)$$

where subscripts *c* and *m* are for calculated and measured values, respectively, derived from the *j*th spectrum recorded at temperature, *T_j*. The two unknowns, *S_c(T₀)* and *E''_c*, which are overdetermined, are adjusted while fitting all the spectrum sets simultaneously. The whole fitting process is iterated until convergence, when the differences between the calculated and observed transmittance spectra are minimized. As described in the initial pseudoline document (<http://mark4sun.jpl.nasa.gov/data/spec/Pseudo/Readme>), when plotting the left-hand side of Eq. (5) vs. (1/*T₀* - 1/*T_j*) and fitting a straight line, the intercept, i.e., the first term in the right hand side of Eq. (5), is the fractional error in the retrieved pseudoline intensity, and the gradient is (*E''_c* - *E''_m*), the error in the currently assumed lower state energy (*E''_c*). For very weak lines whose absorption peaks are close to 100% transmission level, the retrieval of their lower state energies are very sensitive to small uncertainties of the continuum line level, so their lower state energies were constrained to remain within physically reasonable limits during the iterative spectrum fitting.

Finally, a PLL was derived in the HITRAN format (Rothman et al. 2009, 2012) for C₆H₆ absorption features in the respective spectral regions as listed in Table 4. An excerpt of the compiled PLL is presented in Table 6 for N₂-broadened benzene in the Q-branch re-

gion of *v*₄ band. One should note that the molecule index (two digits) has been set to be 73, which is an arbitrary choice. The isotopologue index has been set to be 0 in order to explicitly indicate these parameters are pseudolines rather than true spectroscopic lines. The observed spectra were reproduced using the same pseudoline list, which are presented in Fig. 6. Typical spectral fitting residuals are ~ 3% or better, as shown in Fig. 6. As expected, the residuals are worse for high resolution spectra at low sample pressures (usually for pure benzene spectra, e.g., Fig. 6a), but excellent for pressure-broadened spectra (e.g., Fig. 6b and c). In general, good agreement (better than 3%) was seen across the spectral regions. The strong Q-branch region of the *v*₄ band in the pure benzene spectra at the high spectral resolution (< 0.01 cm⁻¹) showed much larger fitting residuals (~20%) but with no appreciable systematic bias, probably because the 0.005 cm⁻¹ grid spacing does not fully resolve the very fine structure of the Q-branch transitions observed in the low pressure condition. Such poor residuals near the Q-branch become substantially diminished (~3%) in the pressure-broadened spectra as shown in Fig. 5b and d. As seen in Fig. 6c, spurious H₂O absorption features as protruding lines (in blue) are still present in the ratioed spectra. This is because the amount of residual water in the interferometer and in the cold cell varied from spectrum to spectrum, resulting in a significant mismatch in the water absorption peak height. However, in the multispectrum fitting by the pseudolines, the water absorption fitted out, so the resultant benzene pseudolines compiled in this work

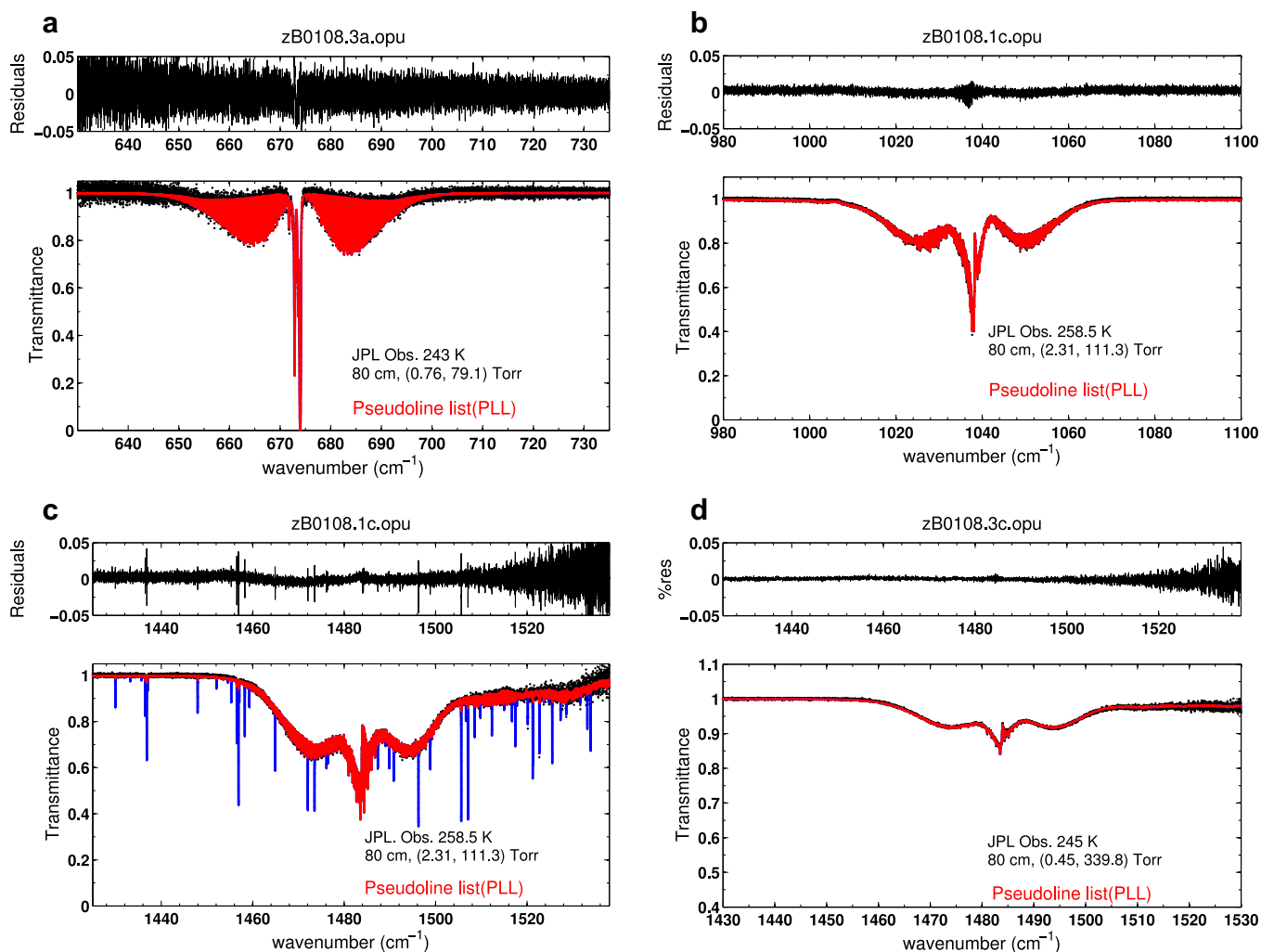


Fig. 6. Residuals, (JPL obs. – calc. based on the pseudoline list) for the N_2 -broadened spectra of benzene (a) in the ν_4 region at 243 K, (b) in ν_{14} region at 258.5 K, (c) and (d) in the ν_{13} region at 258.5 and 245 K, respectively. Better than 3% residuals is seen for all the spectrum sets (except for noisy spectra and the strong Q-branch region). Residual water features arising inside the FT-IR chambers were largely canceled out in these ratioed spectra. As seen in (c), any residual water transitions, from the varying water vapor impurity in the sample, are effectively fitted out during the generation of the benzene pseudoline list.

are almost free of the H_2O line contamination, as shown in the residual plot of Fig. 6c.

Finally, all the results and comparisons are presented for the ν_{14} band region. Synthetic spectra representing Region III (See Table 4) were generated at all the temperatures and pressures of measurements by using one single set of the pseudoline list; they are presented in Fig. 7 with the number of spectra and measurement temperatures captioned on the figures. The noisier features in the residuals are ascribed to spectra with a lower SNR recorded at low pressures (< a few Torr), where absorption features retain much finer structures than the spectrum grid, 0.005 cm^{-1} . All of the N_2 -pressure broadened spectra show fitting residuals better than 1%, which are shown above the spectrum in each panel in Fig. 6.

As part of the evaluation of the pseudoline approach described above, their statistical validity was assessed by inspecting the distribution of lower state energies and line intensities in two ways. Spectroscopic line parameters for the ν_4 band are available in the GEISA 2009 database (Jacquinet-Husson, et al. 2011). A comparison of the pseudolines is illustrated in Fig. 8 to the ‘true’ spectroscopic line parameters for one single cold band, ν_4 , from the GEISA 2009 database. Fig. 8a shows that the mean intensities over 1 cm^{-1} bins for the pseudoline intensities are systematically higher than

their corresponding values from the GEISA 2009 database. However, their intensity variation patterns are very well aligned with each other, indicating that the pseudoline intensities have captured the J and K dependence of the line strengths for the J manifolds. In Fig. 8b, mean intensity-weighted lower state energies over 1 cm^{-1} bins from the benzene pseudolines are compared to those of GEISA. Good agreement is seen in the J-manifold dependence. As expected, the empirical lower state energies for the pseudolines are systematically higher than the values from the GEISA linelist because the pseudolines include all the contributions from cold and hot bands. The empirical lower state energies from the pseudolines should be regarded as effective mean values at the given frequency bin (i.e., pseudoline position), because multiple spectroscopic transitions can occur in the frequency bin, including many of them from hot bands. It is confirmed in Fig. 8b that the propensity of having higher values for the low state energies was picked up well by the pseudoline generation approach.

Recalling that all the 34 spectra were recorded at various pressures and temperatures, any deviation in the spectrum-to-spectrum consistency could be interpreted as an indicator of measurement uncertainties. While performing the multispectrum fitting of the laboratory spectra, we also performed retrieval of VMR Scale Factors (VSF) to speed up the fitting convergence. In an ideal

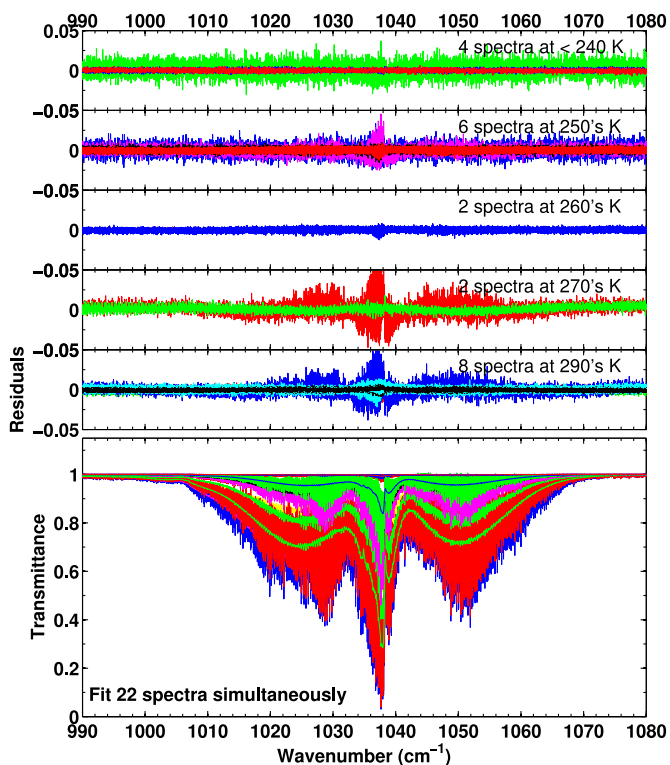


Fig. 7. Each panel shows spectrum fitting residuals for spectral Region III in the range of 5% for the individual experiment conditions, and all the synthetic spectra (in the bottom panel) based on the one single pseudoline list.

condition, *i.e.*, free of noise in the laboratory spectrum, the retrieved VSFs would all be unity, confirming that the known experimental inputs listed in Table 3 are sufficiently accurate. Apart from intrinsic limitations arising from the assumption made for the pseudoline generation (*e.g.*, one representative lower state energy for each given frequency grid), there are several other factors contributing to retrieval error, which includes spectral noise, disturbance on the 100% transmission line, interfering molecules (*i.e.*, residual H₂O), and uncertainties in the experimental conditions (VMR, T, and P). As presented in Fig. 9, the mean value for the retrieved VMR scale factors was observed to be 1.01, *i.e.*, only 1% away from the ideal value when all the bands are considered. Therefore, no significant systematic bias has been observed in the benzene PLL derived from 34 laboratory spectra in this work. For the ν_{14} band, the mean value for the retrieved VMR scale factors was observed to be 1.03, implying a 3% bias, which has been accounted for in the total measurement error estimates.

7. Results and discussions

We have estimated the integrated band intensity, A_B , by summing up the pseudoline strengths over the frequency ranges as listed in Table 4. Since the pseudolines are determined through actual spectrum fitting by adopting a physically sound molecular line shape model, the pseudoline list (PLL) can be used to simulate a spectrum at any other pressures and temperatures within the range of laboratory measurements to better than 5% transmittance. The integrated band intensities, A_B , at 296 K from the N₂-broadened benzene are measured to be 177.0(4.1%), 0.72(10.1%), 14.04(7.3%), 1.38(4.4%), and $27.24(3.4%) \times 10^{-19} \text{ cm}^{-1}/(\text{molecule}\cdot\text{cm}^{-2})$ for the Regions I–V, respectively, as summarized in Table 7. For (H₂+He)-broadened benzene, the integrated band intensity, A_B , for the same ν_4 region specified as Region VI is estimated to be 168.8

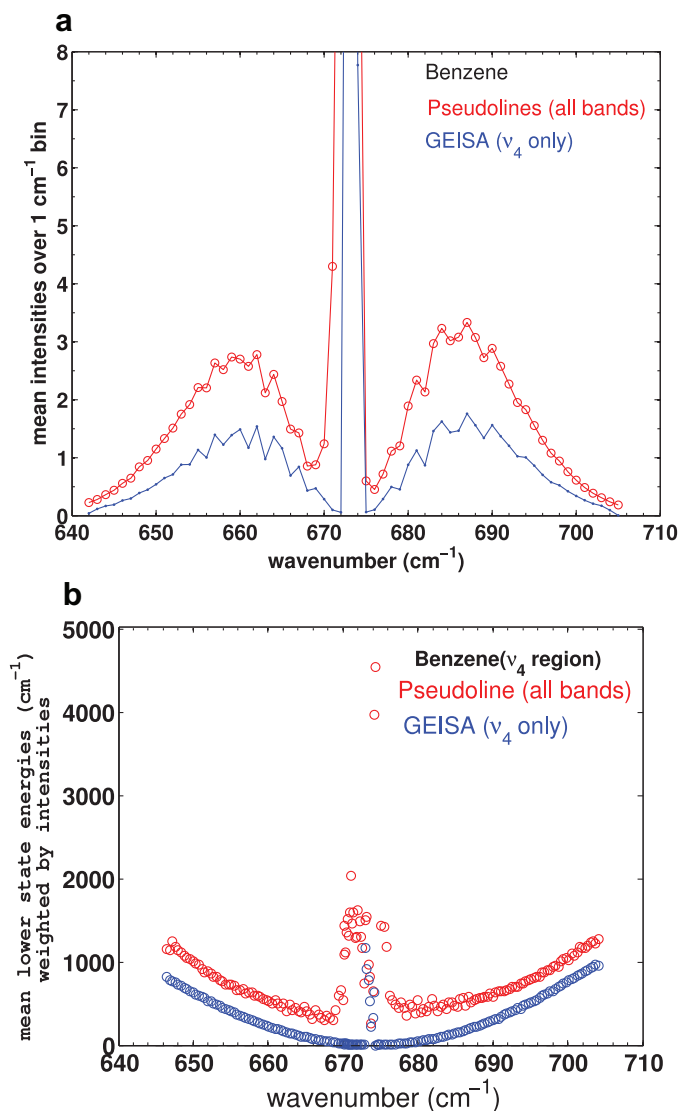


Fig. 8. (a) Mean intensities averaged over 1 cm^{-1} bins for the pseudoline intensities compared to their corresponding values from the GEISA 2009 database. (b) JPL-PLL empirical E'' s averaged over 1 cm^{-1} bin weighted by pseudoline intensities compared to GEISA. The former E'' s are larger, especially near the band center, which can be attributed to contribution from hot band transitions, absent from GEISA.

($1.0\% \text{ cm}^{-1}/(\text{molecule}\cdot\text{cm}^{-2})$), showing a slight discrepancy ($\sim 4.6\%$) from the value derived for N₂-broadened spectra, but consistent within their combined measurement uncertainties. Based on the compiled pseudoline list, combined with the partition function of benzene described in Eq. (4), the integrated band intensities were derived at other temperatures as well, which are presented in Table 7. A small temperature dependence is seen for the derived integrated band intensities, falling by 6 to 15% as temperatures decrease from 296 K to 240 K.

The integrated band intensities derived from the pseudoline list compiled for the N₂-broadened benzene spectra in this work are compared to earlier measurements, as presented in Table 8. Since many of the earlier works reported their intensities at 298 K, we derived the integrated band intensities at 298 K using Eq. (3) in order to facilitate the comparison. There are several other early low resolution measurements, especially for the ν_4 band region, whose integrated band intensities were reported to be 146 (16) at 300 K (Speeding et al. 1956), 140.5(33) at 300 K (Overend 1963), 165.4 (46) at 300 K (Broun and Iogansu 1965),

Table 7
C₆H₆ integrated band intensities, A_B, in 10⁻¹⁹ cm⁻¹/(molecule·cm⁻²) derived from the pseudoline list in the region specified.

Regions	Retrieved from pure- and N ₂ -broadened C ₆ H ₆ spectra Range(cm ⁻¹)	296 K	260 K	250 K	240 K
I (ν ₄ region)	630–735	177.0(4.1%)	170.6(70)	168.9(69)	166.9(68)
II (ν ₁₇ –ν ₂₀)	740–840	0.72(10.1%)	0.48(5)	0.48(5)	0.48(5)
III (ν ₁₄ region)	950–1100	14.04(7.3%)	13.83(10)	13.60(10)	13.28(10)
IV (ν ₇ + ν ₂₀)	1340–1425	1.38(4.4%)	1.31(6)	1.28(6)	1.24(5)
V (ν ₁₃ region)	1425–1538	27.24(3.4%)	24.54(83)	23.80(81)	22.93(78)
Regions	Retrieved from pure- and (85%N ₂ +15%He)-broadened C ₆ H ₆ spectra Range(cm ⁻¹)	296 K	260 K	250 K	240 K
VI (ν ₄ region)	630–735	168.8(1.0%)	160.0(16)	157.1(16)	153.4(15)

Note: Measurement errors reported are estimated by combining retrieval errors for the line intensity parameters and mean value of the Volume Mixing Ratio (VMR) adjusted. See Section 6. for details.

Table 8
Comparison of integrated band intensities, A_B in 10⁻¹⁹ cm⁻¹/(molecule·cm⁻²), at 298 K to the early work available.

C ₆ H ₆	T _{obs} (K)	Region I (ν ₄)	Region III (ν ₁₄)	Region IV (ν ₇ + ν ₂₀)	Region V (ν ₁₃)
This work (C ₆ H ₆ +N ₂)	298	173.9(71)	13.97(102)	1.36(6)	26.17(89)
Rinsland et al. (2008) ^a	298	172.7(52)	14.22(44)	1.25(37)	26.62(80)
PNNL ^b	298.1	172.2	14.22	1.26	26.47
di Lonardo et al (1990) ^c	298	168.8(74)	13.68(29)	1.26(45)	26.18(49)
Raulin et al. (1990) ^d	300	143.9(94)	13.37(61) ^d		23.0(13) ^d
Dang-Nhu et al. 1989	296	171.6(33)			
GEISA	296	159.2 ^e			
Khelifi et al. (1992)	297	152.2			
Goodman et al. (1989)	298		12.42(25) ^d		23.58(80) ^d
Waschull et al. (1997)	295		12.3(10)		

^a From Rinsland et al. (2003)'s absorption cross section in the 615–735 cm⁻¹ region based on the Pacific Northwest National Laboratory (PNNL) spectra at 298 K (Sharpe et al., 2004). However, the contribution from the absorption below 630 cm⁻¹ was insignificant.

^b For the same spectral region, 635–730 cm⁻¹, as for PLL.

^c di Lonardo et al: A_B for ν₄ from pure benzene spectra recorded at 0.03 cm⁻¹ = 165.1(82). We adopted the value from air-broadened spectra of C₆H₆ at 0.05 cm⁻¹, recommended by the author.

^d Cited in Dang-Nhu et al. (1989) and di Lonardo et al. (1999).

^e Report for ν₄ cold band only.

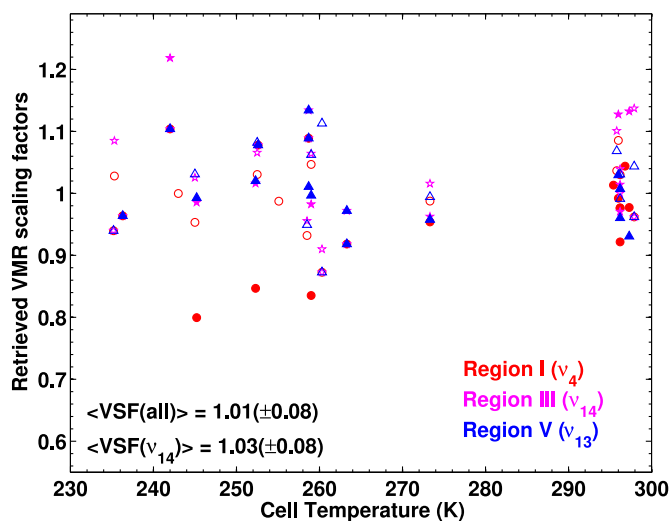


Fig. 9. Volume mixing ratio Scaling Factors (VSF) for benzene retrieved from the observed spectra using the pseudolines are presented for three representative regions. Different colors are for different regions with solid symbols being for pure sample spectra, open symbols for mixtures.

172.7(80) × 10⁻¹⁹ cm⁻¹/(molecule·cm⁻²) at 300 K (Akiyama et al. 1989). Di Lonardo et al. (1999) made an extensive comparison of their results with these earlier measurements, so we do not repeat them in a table. Instead, our measurements have been compared to either recent or more representative values that were employed in the atmospheric remote sensing, as summarized in Table 8.

The reported intensities in the ν₄ region range in the Table 3 of di Lonardo et al. (1999) show a large variation in the integrated band intensities by 23% as shown in Fig. 10a. However, as seen in Fig. 10a and b, our results show an excellent agreement with those from Rinsland et al. (2008), which was based on the PNNL spectrum sets (Sharpe et al., 2004), by 0.7%, -1.8%, -1.7% for the three strongest bands, i.e., Regions I, III, V, respectively. Although the spectral range integrated for Rinsland et al. (2008) was 615–735 cm⁻¹ in contrast to ours (630–735 cm⁻¹), no significant absorption from the out-of-band contribution was observed outside the spectral range specified in Table 7, making it legitimate to do direct comparison for the ν₄ band region. Both results from this work and Rinsland et al. (2008) also show a good agreement with the results from di Lonardo et al (1999) for the ν₄, ν₁₄, and ν₁₃ band regions. However, the results from Raulin et al. (1990) and Khelifi et al. (1992) are significantly lower than the first three works listed in Table 8, including this work.

The GEISA 2009 database compiled spectroscopic line parameters for 9797 transitions for the ν₄ band of benzene for the first time (Jacquinet-Husson et al., 2011), based on the molecular constants and the band strength (S_v) reported by Dang-Nhu et al. (1989) and Dang-Nhu and Pliva (1989). Their integrated intensity in the 642.43–705.26 cm⁻¹ region is computed to be 82.23 × 10⁻¹⁹ cm⁻¹/(molecule·cm⁻²), which is, in fact, for the cold band ν₄ only. Using the vibrational partition function Q_{vib} = 1.810 at 296 K, the integrated band intensity, A_B, for the ν₄ band region including all other contributions from other weak and hot bands in the region can be estimated to be 82.23 × 1.81 = 148.84 × 10⁻¹⁹ cm⁻¹/(molecule·cm⁻²) at 296 K. Since the GEISA database reported for ¹²C₆H₆, whose natural abundance

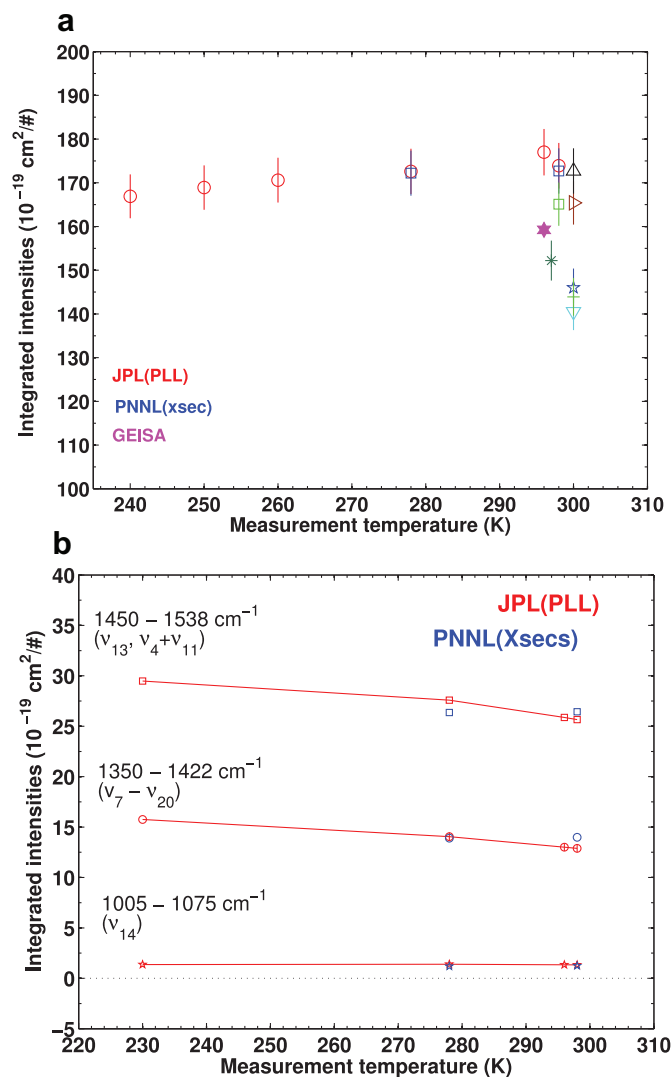


Fig. 10. (a) Our integrated band intensities, labeled as 'JPL(PLL)', at various temperatures are compared to those from Rinsland et al. (2008) labeled as 'PNNL', GEISA, and many other early measurements (See text). di Lonardo et al. 1991 (\square); Spedding and Whiffen 1956 (pentagon); Overend 1963 (inverted triangle); Broun and Iogansen 1965 (right triangle); Akiyama et al. 1989 (triangle); Raulin et al. 1990 (\circ); Khelifi et al. 1992 (\ast). (b). Temperature dependence of the measured integrated band intensities is compared for the selected regions between the results from this work and Rinsland et al. (2008).

is estimated to be 93.48% only, in the normal sample of benzene used in this work, their integrated band intensity should be adjusted for valid comparison with other works, including this study. As a result, the adjusted intensity for a normal sample of benzene becomes $148.84/0.9348 = 159.22 \times 10^{-19} \text{ cm}^{-1}/(\text{molecule}\cdot\text{cm}^{-2})$ at 296 K, which is significantly lower than both this work and Rinsland et al. (2008) by 10% and 6.5%, respectively. Likewise, Dang-Nhu et al. (1989) and Dang-Nhu and Pliva (1989), which were cited in the GEISA database, reported the C_6H_6 v_4 band intensity, $S_v = 218.5 (\pm 4.5) \text{ cm}^{-1}/\text{atm}$ at 296 K, from which one can deduce the integrated band intensity (A_B) ($\text{cm}^{-1}/(\text{molecule}\cdot\text{cm}^{-2})$) of normal sample of benzene (C_6H_6) in the v_4 band region to be $159.5(3.3) \times 10^{-19} \text{ cm}^{-1}/(\text{molecule}\cdot\text{cm}^{-2})$ using Eq. (6),

$$A_B = S_v \times Q_{\text{vib}}(T_0) \times T_0 / 7.3391 \times 10^{21} \quad (6)$$

where $Q_{\text{vib}} = 1.810$ computed at $T_0 = 296 \text{ K}$ by Eq. (4). As expected, the value reported by Dang-Nhu et al. (1989) and Dang-Nhu and Pliva (1989) was in good agreement with the GEISA value, thus

their measurement is lower than both this work and Rinsland et al. (2008) as discussed above.

We have estimated error budgets considering the uncertainties associated with the experimental conditions, e.g., measurement temperature drifts, path length of the gas cells, pressure readings, zero-offsets, 100% transmission level offsets due to possible ice absorption features, and uncertainty in the mixing ratio for the admixture gas samples. Among them the last two are the biggest contributors to the error. Firstly, an offset from the 100% transmission level caused by extra absorption by unidentified cryodeposits on the windows, growing with time during which the cell was kept cold, was minimized to be less than 0.5–1% by taking the average of two empty spectra recorded before and after the sample scans. Secondly, as presented in Fig. 9, the mean value of the retrieved volume mixing ratio scale factors (VSFs) for all the spectral fitting regions shows only 1% offset. The 1% offset could be taken as an overall measurement error with respect to the experimental inputs while their standard deviation, 8%, reflects the retrieval noise from spectrum to spectrum that is primarily governed by spectral noise (i.e., S/N). The mean values of the VSF, i.e., systematic bias with respect to the experimental inputs, were observed to be -1.0% , 0.4% , 7% , 3% , 3% , and 0.8% for Regions I–VI, respectively. Since the pseudoline intensity retrievals were affected by these offsets, we have estimated measurement uncertainties to be 4.1%, 10.1%, 7.3%, 4.4%, 3.4%, and 1.0% for the integrated band intensities in the six Regions, I–VI, respectively, by combining the mean value of the VSF's and the retrieval uncertainties for the pseudoline intensities, which are listed in Table 7.

One should keep in mind that the pseudoline list represents total apparent absorption with all contributions from cold-, hot-, and other weak bands integrated. For polyatomic molecules having significant number of low-lying states well below 1000 cm^{-1} , their hot bands persist even in the cold temperatures such as $\sim 230 \text{ K}$ in the Titan's stratosphere. Benzene is worse, because it will mostly condense out before the ambient temperature is sufficiently cold to suppress the hot band contributions. Therefore, in order to achieve the decent precision in the spectroscopic observations, characterization of the hot band features cannot be put aside. This point is well illustrated in Fig. 11, where synthetic spectra based on both the pseudoline list from this work and traditional spectroscopic linelist of the v_4 band from the GEISA 2009 database (Husson-Jacquinet et al. 2013) are compared; the missing contribution from hot and weak combination band features are substantial not only at 296 K, but also at a cold temperature, 235 K. This is critical for the accurate analysis of spectral regions in the observed atmospheric spectrum, particularly for the region congested with absorption features from many other atmospheric molecules. The PLL generated from this work enables a more accurate estimation of the atmospheric abundance of benzene. Furthermore, the pseudoline list can reproduce the expected hot band features well, so as to keep the unfitted featureless broadband features from being misinterpreted as the effect of aerosols and scattering. Moreover, as pointed out by Nixon et al. (2009), accurate interpretation and a search for new trace gases appearing in the CIRS spectra become challenging without proper characterization of polyatomic species (e.g., benzene at $15 \mu\text{m}$).

Lastly, it is worthwhile to discuss error estimates expected when these pseudolines are extrapolated to extreme conditions, e.g., at temperatures as cold as 60 K. As pointed out earlier, the pseudoline list is readily amenable to line-by-line calculations for radiative transfer modeling to other pressure and temperature conditions. Thus, we have estimated the integrated band intensities, A_B , for the Region I (v_4 band region) at temperatures between 260 and 60 K respectively from the pseudoline lists and compared to the values from the GEISA 2009 database having their v_4 band line list as a canonical comparison set representing true spectroscopic

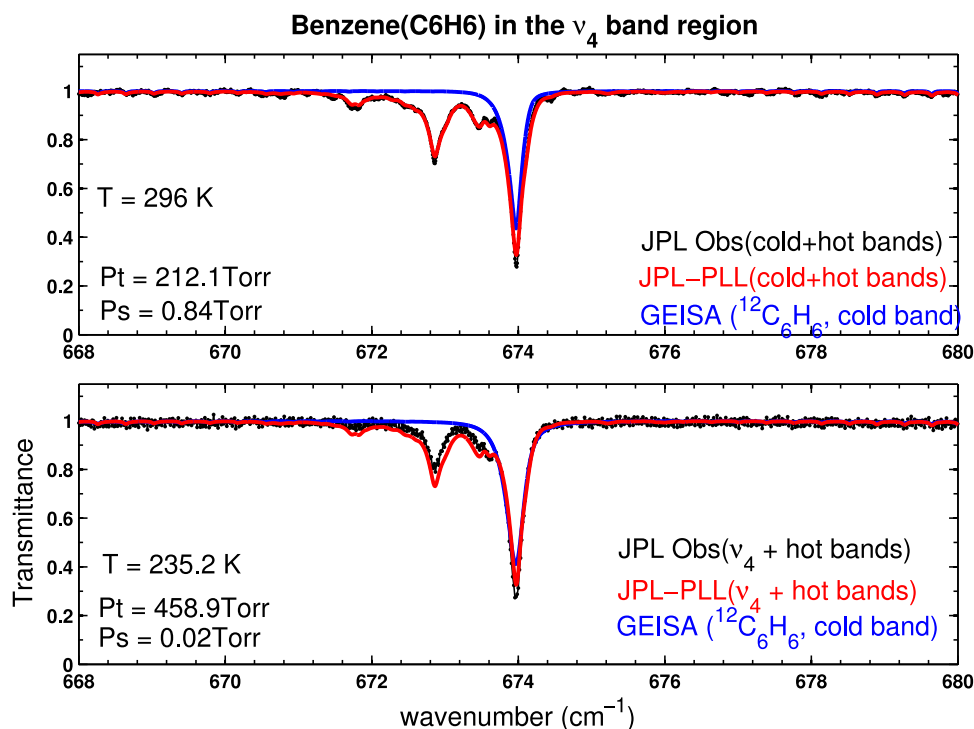


Fig. 11. Comparison of calculated spectra for the ν_4 region. Synthetic spectra from GEISA spectroscopy (blue) and from pseudo-linelist (red) are compared to the corresponding observed spectra (black). It shows that the PLL nicely reproduces the observed hot- and cold-band features in the upper and lower panels, respectively.

line parameters. It is encouraging to observe that the integrated band intensities estimated from the pseudolines show agreement within $\sim 12\%$ for the N_2 -broadened benzene pseudoline and $\sim 34\%$ for (H_2+He) -broadened spectra at the temperatures between 260–60 K when further adjustment was made to the GEISA values by 10% and $\sim 6\%$, respectively, to compensate the discrepancy already observed at 296 K. The reasonable agreement for the extrapolation of the pseudoline list to the extreme temperatures indicates that the empirical lower state energies derived through multispectrum fitting are sufficiently good to represent the line intensity variation with temperatures. It should be recalled that, since the benzene vapor pressures, whose information is not available at the temperatures below 200 K, but is expected to be extremely small at colder temperature, e.g., 100 K, several kilometers of absorption path would be needed to study benzene spectroscopy at these temperatures.

8. Conclusions

High-resolution laboratory characterization of the benzene spectroscopic features at cold temperatures is required to accurately interpret the spectroscopic observations from past, present and future planetary missions (ISO/SWS, Cassini/CIRS, JUNO/JUICE, etc.), thus providing better constraints for hydrocarbon photochemistry modeling. We have therefore measured absorption cross sections for N_2 -broadened benzene (C_6H_6) spectra in the 690–1550 cm^{-1} region at temperatures from 235 K to 297 K and created a pseudoline list (PLL) that represents the measured spectra to within 5%. We also have retrieved a separate PLL for the pre-mixture (85% H_2 +15% He) broadened benzene in the 630–735 cm^{-1} region. The pseudoline list includes the line strengths, and lower state energy, as well as other prescribed parameters (frequency bins as line center positions, pressure-broadened line widths and their temperature dependence, and pressure-induced frequency shifts) assumed for the line shape model of Voigt profile. It is ob-

served that the pseudoline set could reproduce better the observed spectral absorption, i.e., well within 3% at any of the temperature and pressure conditions for the pressure-broadened spectra, except for the strong Q-branch of the ν_4 band at 674 cm^{-1} . Total integrated band intensity in the 690–1550 cm^{-1} region is estimated to be $2.204(\pm 93) \times 10^{-17} \text{ cm}^{-1}/(\text{molecule}\cdot\text{cm}^{-2})$ at 296 K derived from the N_2 -broadened absorption features, which is in an excellent agreement (better than 0.5%) with the earlier low-resolution N_2 -broadened benzene measurements (Rinsland et al., 2008; Sharpe et al., 2004).

We have compiled the pseudoline lists for each of the five spectral regions in an electronic file by adopting the HITRAN format (a sample is shown in Table 6). The two separate lists of C_6H_6 pseudolines have been generated; one for N_2 -broadened spectra in the five spectral regions, and the other for (H_2+He) -broadened spectra in the ν_4 band region. The PLL for the five strongest regions (Regions I, III–VI) are reported in electronic supplements and also will be available from: (<http://mark4sun.jpl.nasa.gov/data/spec/Pseudo>). They can readily be used in the line-by-line radiative transfer calculations in the same manner as for true spectroscopic line parameters. In modeling atmospheres, the pseudoline approach benefits the spectroscopic analysis of atmospheric molecules, such as benzene, whose spectroscopic line parameters are yet to be accounted for in any quantum mechanics analysis. The pseudoline approach, however, should be regarded as a practical interim solution until quantum-mechanically-based spectroscopic line parameters are available.

Acknowledgments

Research described in this article was performed at the Jet Propulsion Laboratory, California Institute of Technology, under contracts and cooperative agreements with the National Aeronautics and Space Administration.

Supplementary materials

Supplementary material associated with this article can be found, in the online version, at doi:10.1016/j.icarus.2016.01.012.

References

- Akiyama, M., Shimizu, Y., Itaya, H., et al., 1989. Charge-distribution on benzene determined from infrared band intensities by a new equation. *J. Phys. Chem.* 93, 2280–2284.
- Anderson, P.W., 1949. Pressure broadening in the microwave and infrared regions. *Phys. Rev.* 76, 647–661.
- Bézar, B., Drossart, P., Encrenaz, T., et al., 2001. Benzene on the giant planets. *Icarus* 154, 492–500.
- Blass, W.E., Halsey, W.E., Jennings, D.E., 1987. Self-gas and foreign-gas broadening of ethane lines determined from diode-laser measurements at 12 μm . *J. Quant. Spectrosc. Radiat. Transf.* 38, 183–184.
- Booth, R.S., Brault, J.W., Labeyrie, A., 1985. High resolution in astronomy. Saas Fee Courses 15. Geneva Observatory, CH-1290, Sauverny, Switzerland.
- Breeze, J.C., Ferriso, C.C., Ludwig, C.B., et al., 1965. Temperature dependence of the total integrated intensities. *J. Chem. Phys.* 42, 402–406.
- Broun, E.V., Iogansen, A.V., 1965. Intensity of ν_4 benzene band in gas phase and in solutions. *Opt. Spectrosc.* 18, 348–349.
- Cane, E., Miani, A., Trombetti, A., 1997. The ν_6 , ν_7 , ν_8 , and ν_{19} gas phase fundamental frequencies of $^{12}\text{C}_6\text{H}_6$. *Chem. Phys. Lett.* 272, 83–85.
- Cernicharo, J., Heras, A.M., Tielens, A.G.G.M., et al., 2001. Infrared space observatory's discovery of C_4H_2 , C_6H_2 , and benzene in CRL 618. *Astrophys. J.* 546, L123–L126.
- CHEERIC 2015 (Chemical Engineering Research Information Center), Korea Thermo-physical Properties data Bank.
- Coustenis, A., Salama, A., Schulz, B., Ott, S., et al., 2003. Titan's atmosphere from ISO mid-infrared spectroscopy. *Icarus* 161, 383–403.
- Coustenis, A., Jennings, D., Jolly, A., et al., 2008. Detection of C_2HD and the D/H ratio on Titan. *Icarus* 197, 539–548. doi:10.1016/j.icarus.2008.06.003.
- Coustenis, A., Jennings, D.E., Nixon, C.A., et al., 2010. The composition of Titan's stratosphere from Cassini/CIRS mid-infrared spectra. *Icarus* 207, 461–476.
- Crawford Jr., B., 1958. Vibrational intensities: integration theorems. *J. Chem. Phys.* 29, 1042–1045.
- Cui, J., 12 colleagues, 2009. Analysis of Titan's neutral upper atmosphere from Cassini Ion Neutral Mass Spectrometer measurements. *Icarus* 200, 581–615.
- Dang-Nhu, M., Blanquet, G., Walrand, J., et al., 1989. Spectral intensities in the ν_4 band of benzene at 15 μm . *J. Mol. Spectrosc.* 134, 237–239.
- Dang-Nhu, M., Pliva, J., 1989. Intensities in the ν_4 , ν_{12} , ν_{13} , and ν_{14} bands of benzene. *J. Mol. Spectrosc.* 138, 423–429.
- di Lonardo, G., Fusina, L., Masciarelli, G., et al., 1999. Integrated band strengths of benzene vapour in the 600 – 1900 cm^{-1} region. *Spectrochim. Acta Part A* 55, 1535–1544.
- Doskey, P.V., Gaffney, J.S., 1992. Non-methane hydrocarbons in the Arctic atmosphere at Barrow Alaska. *Geophys. Res. Lett.* 19, 381–384.
- Drouin, B.J., Yu, S., Elliott, B.M., Crawford, T.J., Miller, C.E., 2013. High resolution spectral analysis of oxygen. III. Laboratory investigation of the airglow bands. *J. Chem. Phys.* 139, 1–11 Article no. 144301.
- Goodman, L., Ozkabak, G., Wiberg, K.B., 1989. The benzene ground-state potential surface 4. Discrimination between multiple E_{1u} forced-field solutions through infrared intensities. *J. Chem. Phys.* 91, 2069–2080.
- Herzberg, G., 1968. *Infrared and Raman Spectra*, vol. 2, 13th ed. Princeton, NJ.
- Jacquinet-Husson, N., Crepeau, L., Armante, R., et al., 2011. The 2009 edition of the GEISA spectroscopic database. *J. Quant. Spectrosc. Radiat. Transf.* 112, 2395–2445.
- Jennings, D.E., 10 colleagues, 2008. Isotopic ratios in Titan's atmosphere from Cassini CIRS limb sounding: HC_3N in the North. *Astrophys. J.* 681, L109–L111.
- Kekulé, F.A., 1890. Benzolfest: Rede. *Berichte der Deutschen Chemischen Gesellschaft* 23, 1302–1311. doi:10.1002/cber.189002301204, English translation: Wilcox D.H., Greenbaum, F.R., 1965. *Kekulé's benzene ring theory: A subject for lighthearted banter*. *J. Chem. Edu.* 42, 266–67. DOI:10.1021/ed042p266).
- Khlifi, M., Raulin, F., Dang-Nhu, M., 1992. Benzene ν_4 integrated band intensity versus temperature. *J. Mol. Spectrosc.* 154, 235–239.
- Kim, S.J., Caldwell, J., Rivalvo, A.R., et al., 1985. Infrared polar brightening on Jupiter. *Icarus* 64, 233–248.
- Lide, D.R., 1998. *CRC Handbook of Chemistry and Physics*, 79th ed. CRC Press, New York.
- Lide, D.R., 2011. *CRC Handbook of Chemistry and Physics*, 92th ed. CRC Press, New York.
- Lindenmayer, J., Magg, U., Jones, H., 1988. Diode laser spectroscopy of the ν_4 band of benzene. *J. Mol. Spectrosc.* 128, 172–175.
- Margolis, J.S., 1990. Empirical values of the ground state energies for methane transitions between 5500 and 6150 cm^{-1} . *Appl. Opt.* 29, 2295–2302.
- Miani, A., Cane, E., Palmieri, P., et al., 2000. Experimental and theoretical anharmonicity for benzene using density functional theory. *J. Chem. Phys.* 112, 248–259.
- Moses, J.I., Bezard, B., Lellouch, E., et al., 2000. Photochemistry of Saturn's atmosphere. I. Hydrocarbon chemistry and comparison with ISO observations. *Icarus* 143, 244–298.
- Moses, J.I., Greathouse, T.K., 2005. Latitudinal and seasonal models of stratospheric photochemistry on Saturn: Comparison with infrared data from IRTF/TEXES. *J. Geophys. Res.* 110. doi:10.1029/2005JE002450.
- Niemann, H.B., Atreya, S.K., Carignan, G.R., et al., 1998. Chemical composition measurements of the atmosphere of Jupiter with the Galileo Probe mass spectrometer. *Adv. Space Res.* 21, 1455–1461.
- Nixon, C.A., Jennings, D.E., Flaud, J.-M., et al., 2009. Titan's prolific propane: The Cassini CIRS perspective. *Planet. Space Sci.* 57, 1573–1585.
- Overend, J., 1963. *Infra-Red Spectroscopy and Molecular Structure: An Outline of the Principles*. In: Davies, M. (Ed.) Elsevier, New York, p. 368 Cited in *Di Lonardo G, Fusina L, Masciarelli G, Tullini F, 1999. Integrated band strengths of benzene vapour in the 600 – 1900 cm^{-1} region. Spectrochimica Acta Part A. 55, 1535 – 1544.*
- Pliva, J., Johns, J.W.C., 1983. The ν_{13} fundamental band of benzene. *Can. J. Phys.* 61, 269–277.
- Pliva, J., Johns, J.W.C., 1984. The perpendicular band ν_{13} of benzene near 10 μm fundamental band of benzene. *J. Mol. Spectrosc.* 107, 318–323.
- Pliva, J., Johns, J.W.C., Goodman, L., 1989. Infrared bands of $^{13}\text{C}_6\text{H}_6$: ν_{13} and ν_{14} . *J. Mol. Spectrosc.* 134, 227–233.
- Pliva, J., Johns, J.W.C., Goodman, L., 1991. Infrared bands of isotopic benzenes: ν_{13} and ν_{14} of $^{13}\text{C}_6\text{H}_6$. *J. Mol. Spectrosc.* 148, 427–435.
- Pliva, J., Johns, J.W.C., Lu, Z., 1993. High-resolution study of the difference band $\nu_{17} - \nu_{20}$ of benzene. *J. Mol. Spectrosc.* 161, 269–274.
- Poltoratskii, G.M., 1962. Dampfdruck von Benzol bei Temperaturen 11–40°C. *Zh. Prikl. Khim* 35, 1638–1640.
- Raulin, F., Mourey, D., Toupance, G., 1982. Organic syntheses from $\text{CH}_4\text{-N}_2$ atmospheres: implications for Titan. *Orig. Life* 12, 267–279.
- Raulin, F., Accaoui, B., Razaghi, A., et al., 1990. Infrared spectra of gaseous organics: application to the atmosphere of Titan – II. Infrared intensities and frequencies of C_4 alkanenitriles and benzene. *Spectrochim. Acta.* 46A, 671–683.
- Rinsland, C.P., Devi, M.V., Blake, T.A., et al., 2008. Quantitative measurement of integrated band intensities of benzene vapor in the mid-infrared at 278, 298, and 323 K. *J. Quant. Spectrosc. Radiat. Transf.* 109, 2511–2522.
- Rothman, L.S., Gordon, I.E., Barbe, A., et al., 2009. The HITRAN 2008 molecular spectroscopic database. *J. Quant. Spectrosc. Radiat. Transf.* 110, 533–572.
- Rothman, L.S., Gordon, I.E., Babikov, Y., et al., 2013. The HITRAN 2012 molecular spectroscopic database. *J. Quant. Spectrosc. Radiat. Transf.* 130, 4–50.
- Sharpe, S., Johnson, T., Sams, R., et al., 2004. Gas-phase data bases for quantitative infrared spectroscopy. *Appl. Spectrosc.* 58, 1452–1461.
- Snively, D.L., Walters, V.A., Colson, S.D., et al., 1984. FTIR spectrum of benzene in a supersonic expansion 103, 423–429.
- Spedding, H., Whiffen, D.H., 1956. Intensities in the infrared spectrum of benzene. *Proc. R. Soc. Lond. A* 238, 245–255.
- Sung, K., Toon, G.C., Mantz, A.W., et al., 2013. FT-IR measurements of cold C_3H_8 cross sections at 7–15 μm for Titan atmosphere. *Icarus* 226, 1499–1513.
- Thompson, W.R., Henry, T.J., Schwartz, J.M., et al., 1991. Plasma discharge in $\text{N}_2 + \text{CH}_4$ at low pressures; experimental results and applications to Titan. *Icarus* 90, 57–73.
- Toon, G.C., Farmer, C.B., Scharper, P.W., et al., 1992. Composition measurements of the 1989 Arctic winter stratosphere by airborne infrared solar absorption spectroscopy. *J. Geophys. Res.* 97, 7939–7961.
- Toon, G.C., Blavier, J.F., Sen, B., et al., 1999. Comparison of Mk-IV balloon and ER-2 aircraft measurements of atmospheric trace gases. *J. Geophys. Res.* 104, 26779–26790.
- Varanasi, P., Chudamani, C.S., 1989. Measurements of collision-broadened line widths in the 7.66- μm band of at temperatures relevant to the Atmosphere. *J. Geophys. Res.* 94, 13073–13078.
- Vuitton, V., Yelle, R.V., Cui, J., 2008. Formation and distribution of benzene on Titan. *J. Geophys. Res.* 113 (E5), E05007. doi:10.1029/2007JE002997.
- Waite, J.H., Young, D.T., Craven, T.E., et al., 2007. The process of tholin formation in Titan's upper atmosphere. *Science* 316 (5826), 870–875.
- Waschull, J., Sumpf, B., Heiner, Y., et al., 1995. Diode laser spectroscopy in the ν_{14} band of benzene. *Infra. Phys. Tech.* 37, 193–198.
- Waschull, J., Heiner, Y., Sumpf, B., et al., 1997. Diode laser spectroscopy in the 9.8 μm ν_{14} band of benzene. *J. Mol. Spectrosc.* 184, 434–441.
- Waschull, J., Heiner, Y., Sumpf, B., et al., 1998. Diode laser spectroscopy in the 9.8 μm ν_{14} band of benzene. II. Self-, Air-, and Nobel-Gas broadening coefficients. *J. Mol. Spectrosc.* 190, 140–149.
- Wilson, E., Atreya, S.K., Coustenis, A., 2002. Mechanisms for the formation of benzene in the atmosphere of Titan. *J. Geophys. Res.-Planets* 108. doi:10.1029/2002JE001896.
- Wilson, E.H., Atreya, S.K., Coustenis, A., 2003. Mechanism for the formation of benzene in the atmosphere of Titan. *J. Geophys. Res.* 108, 5014. doi:10.1029/2002JE001893.
- Wilson, E.H., Atreya, S.K., 2004. Current state of modeling the photochemistry of Titan's mutually dependent atmosphere and ionosphere. *J. Geophys. Res.* 109. doi:10.1029/2003JE002181. E06002.
- Wong, A.-S., Lee, A.Y., Yung, Y.L., et al., 2000. Jupiter aerosol chemistry in the polar atmosphere. *Astrophys. J.* 534, L215–L217.
- Wong, A.-S., Yung, Y.L., Friedson, A.J., 2003. Benzene and Haze formation in the polar atmosphere of Jupiter. *Geophys. Res. Lett.* 30. doi:10.1029/2002GL016661.
- Yoon, H.H., Horst, S.M., Hicks, R.K., et al., 2014. The role of benzene photolysis in Titan haze formation. *Icarus* 233, 233–241.
- Yung, Y.L., Allen, M., Pinto, J.P., 1984. Photochemistry of the atmosphere of Titan: Comparison between model and observations. *Astrophys. J. Suppl.* 55, 465–506.